Bonding Environments and Radiation Stabilities of Phosphate Glasses

Nuclear Fuel Cycle and Supply Chain

Prepared for U.S. Department of Energy

J. Marcial,^(a) S. Chong,^(a) B.J. Riley,^(a) R.K. Brow,^(b) J.D. Vienna,^(a) C.W. Kim,^(c) and M. Tang^(d)

(a) Pacific Northwest National Laboratory, (b) Missouri University of Science and Technology, (c) MoSci Corporation, (d) U.S. Department of Energy Office of Nuclear Energy

> March 19, 2024 PNNL-35754



DISCLAIMER

This information was prepared as an account of work sponsored by an agency of the U.S. Government. Neither the U.S. Government nor any agency thereof, nor any of their employees, makes any warranty, expressed or implied, or assumes any legal liability or responsibility for the accuracy, completeness, or usefulness, of any information, apparatus, product, or process disclosed, or represents that its use would not infringe privately owned rights. References herein to any specific commercial product, process, or service by trade name, trade mark, manufacturer, or otherwise, does not necessarily constitute or imply its endorsement, recommendation, or favoring by the U.S. Government or any agency thereof. The views and opinions of authors expressed herein do not necessarily state or reflect those of the U.S. Government or any agency thereof.

SUMMARY

Phosphate glasses have a wide range of commercial and industrial uses due to their unique optical, chemical, and physical properties. They are a candidate material for use as an advanced waste form matrix for immobilizing radioactive waste due to their unique ability to immobilize high fractions of alkali- and sulfur-rich streams in chemically durable glasses. This literature review provides an overview of the structure of phosphate glasses, waste-form related properties of interest (e.g., chemical durability and radiation stability), a summary of how specific composition ratios affect chemical durability (e.g., [Fe]/[P] ratio, [O]/[P] ratio, Fe²⁺/Fe³⁺ ratio), as well different ways that phosphate glasses can be affected by radiation. All of these properties are of interest to the waste form community as phosphate glasses, primarily Fe-P-O glasses, are investigated for usage in immobilizing various types of nuclear waste. Possible uses include U.S. legacy wastes as well as salt-based high-level wastes from molten salt reactors and pyroprocessing of used nuclear fuels.

CONTENTS

SUN	MMARY	iii
1.	INTRODUCTION	1
2.	PHOSPHATE GLASS STRUCTURE-PROPERTY RELATIONSHIPS 2.1 Short-Range Ordering in Phosphate Glasses 2.2 Medium-Range Ordering in Phosphate Glasses 2.3 Iron Phosphate Glasses for Nuclear Waste Remediation 2.4 Dissolution Behavior of Phosphate Glasses	3 4 7
3.	RADIATION TOLERANCE	16
4.	SUMMARY AND CONCLUSIONS	25
5.	ACKNOWLEDGEMENTS	26
6.	REFERENCES	27
	ure 2-1. Description of the bonding character of phosphate systems. "VU" denotes valence units. ure 2-2. (a) ³¹ P MAS NMR of xNa ₂ O-(1-x)P ₂ O ₅ glasses with varying additions of Na ₂ O demonstrating the spectroscopic signatures of Q ² and Q ³ species at -20 and -51 ppm and (b) the quantified fraction of Q ² and Q ³ species, denoted as f(Q"), as a function of Na ₂ O addition with lines provided to guide the eye. This figure was modified from the original (Brow et al. 1994)	
Figu	modified from the original (Brow et al. 1994)	4
Figu	originals (Brow et al. 1995; Sales et al. 1998; Brow 2000)	
Figu	are 2-5. (a) Effect of the [O]/[P] ratio on the average PO ₄ -anion chain length in polyphosphate glasses (see Figure 2-4) and the average charge per chain due to the presence of terminal NBO. (b) Summary of iron phosphate glass dissolution rate as a function of time for different Fe:P molar ratios at a fixed [O]/[P] of 3.40±0.03 and (c) the semilog plot of log[NL(P)] vs the Fe:P molar ratio (Ma et al. 2017)	
Figu	are 2-6. HPLC chromatographs for $xNa_2O \cdot xCaO \cdot (1-2x)P_2O_5$ polyphosphate glasses where the $[O]/[P]$ ratio was (a) 3.44, (b) 3.29, (c) 3.17, (d) 3.09, (e) 3.04, or (f) 3.01.	

The chain lengths are provided next to the relevant peaks. This figure was modified from the original (Ma et al. 2018)	7
Figure 2-7. (top) Liquidus surface for the Fe(PO ₃) ₃ ·Fe ₂ O ₃ system exhibiting the glass- forming range of interest nuclear waste iron phosphate glasses (Brow et al. 2019). (bottom) Liquidus surface for the Fe(PO ₃) ₃ ·Fe ₄ (P ₂ O ₇) ₃ compositional range which of interest for nuclear waste immobilization.	8
Figure 2-8. Compiled dissolution rates for phosphate glasses mixed with various simulated waste compositions as a function of [O]/[P] ratio. This figure was modified from the original by Day et al. (Day and Ray 2013)	9
Figure 2-9. Graphical representations of (a) octahedral coordination and (b) tetrahedral coordination environments commonly found for Fe ²⁺ /Fe ³⁺ .	9
Figure 2-10. Summary of Mössbauer spectroscopy of $15Cs_2O \cdot yMoO_3 \cdot (28.75-y)Fe_2O_3 \cdot 56.25P_2O_5$ glasses showing Fe^{2^+} and Fe^{3^+} in glasses with similar targeted composition batched with either (a) H_3PO_4 or (b) $NH_4H_2PO_4$. The regions representing Fe^{2^+} and Fe^{3^+} species are labeled accordingly. The Fe^{2^+} concentration (from total Fe , i.e., $Fe^{2^+} + Fe^{3^+}$) measured in (a) and (b) were 5 mass% and 53 mass%, respectively. This figure was modified from the original (Bai et al. 2020)	. 10
Figure 2-11. (a-c) HPLC of sodium-iron phosphate glasses with different [O]/[P] ratios of (a) 3.51, (b) 3.43, and (c) 3.27. (d) Schematic of the general structure of sodium iron phosphate glasses. This figure was modified from the original by Ma and Brow (2014).	.11
Figure 2-12. (a) normalized mass release (mg/cm²) values for sodium, calcium, and phosphorus and (b) pH of the leachate solutions for static dissolution of x Na ₂ O· x CaO· $(1-2x)$ P ₂ O ₅ glasses at room temperature as functions of time and [O]/[P] molar ratios, which are shown as the numbers on all datasets in (a) and (b). These figures were modified from the originals by Ma et al. (2018)	.12
Figure 2-13. (a) General processes for glass dissolution [modified from the original by Vienna et al. (2013)]. (b-d) Schematic representation of the mechanism for the ingress of water into phosphate glasses and the subsequent leaching of hydrated ions into solution.	.13
Figure 2-14. Normalized mass release of P, Na, and Fe as a function of time for glasses with (a) $[O]/[P] = 3.4$ and (b) with $[O]/[P] = 3.12$. This figure was modified from the original by Ma et al. (2017).	.14
Figure 2-15. (a) Mass fraction of dissolved phosphorus $[\alpha(P)]$ as a function of time with two fit lines provided for DM (3D diffusion domain, proportional to $t^{1/2}$) and CVM (contracting volume domain, proportional to t). (b) Isosurface plot showing the compositional dependence of the rate parameter for the 3D diffusion model (k_1). These figures were modified from the original (Ma et al. 2017)	.15
Figure 3-1. (a-d) Schematic representations of some radiation induced defects in phosphate glasses (this figure was modified from the original by Ebeling et al. (2002) and more information about each of these is provided in Table 3-1). (e) Different locations of radiation-induced absorption bands in phosphate glasses in terms of both wavelength and hv including phosphate bonded oxygen hole centers (POHCs), phosphate-related electron centers (PECs), and oxygen related hole centers (OHCs). This figure was modified from the original by He et al. (2017b)	. 17

Figure 3-2. Scanning electron micrographs of iron phosphate glasses showing (a) as-made samples and (b) after He ion irradiation on a pre-damaged specimen. This figure was modified from the original by Dube et al. (2016)	20
Figure 3-3. (a,b) Bright-field transmission electron micrographs (TEM) on iron phosphate glasses without Na in the structure (a) and with Na in the structure (b) after irradiation by electron beam at different doses. (c) Pseudocolored elemental energy dispersive X-ray spectroscopy dot maps of P, Fe, and O using energy-filtered TEM on aluminophosphate glass irradiated to different electron doses. This figure was modified from the original by Sun et al. (2005).	21
Figure 3-4. (a) Photographs of a series of phosphate-based glasses with different H_3BO_3 :SiO ₂ mass ratio (0:2, 1.5:2, 4.5:2 and 7.5:2) after exposure to different cumulative (cumul.) radiation doses of 20, 100, 250, 500, or 1000 krad(Si). (b) Transmittance spectra of the series of glasses with different mass ratios of H_3BO_3 :SiO ₂ (see above) after γ irradiations of 500k rad(Si) after being aged for 165 h. (c) transmittance spectra of the H_3BO_3 :SiO ₂ = 0:2 sample after irradiations of 20, 100, 250, 500, and 1000 krad(Si) with an aging time of 165 h. (d) Transmittance spectra of the sample (H_3BO_3 :SiO ₂ = 0:2) with γ radiation of 500 krad(Si) after different aging times of 0, 15, 65, 165, 365, 765, or 1500 h at room temperature. This figure was modified from the original by He et al. (2017b)	22
TABLES	
Table 1-1. Example of events regarding phosphate waste form development technologies	2
Table 3-1. Different types of radiation-induced defects based on a work by Ebeling et al. (2002) including optical information for each (EPR = electron paramagnetic resonance, EC = electron center; HC = hole center).	18
Table 3-2. Summary of some radiation effect studies of the phosphate glasses in the literature. (a)Simulation only; (b)the exact composition was not provided in the paper; "—" means that the data was not provided in the primary reference	19

March 19, 2024 ix

ACRONYMS AND ABBREVIATIONS

AZS alumina-zirconia-silicate

BO bridging oxygen BSG borosilicate glass

CVM contracting volume model

DFC Denver fireclay DM diffusion model

DOE-EM Department of Energy Office of Environmental Management

DOE-NE Department of Energy Office of Nuclear Energy

DST double-shell tank

DWPF Defense Waste Processing Facility

EC electron center

EDTA ethylenediaminetetraacetic acid

HC hole center

HLW high-level nuclear waste

HPLC high-pressure liquid chromatography

IFR Integral Fast Reactor LAW low-activity waste

LMFBR liquid metal fast breeder reactor

LRO long-range ordering

MAS NMR magic angle spinning nuclear magnetic resonance

MRO medium-range ordering

MUST Missouri University of Science and Technology^a

NAP sodium-aluminophosphate NBO non-bridging oxygen

NEUP Nuclear Energy University Partnership

OHC oxygen-hole centers

PAMELA Pilot Anlage Mol zur Erzeugung Lagerfähiger Abfälle

PEC phosphate-related electron centers PNL Pacific Northwest Laboratory

PNNL Pacific Northwest National Laboratory POHC phosphorous-oxygen hole centers

R.O.K. Republic of Korea
SAP silica aluminophosphate
SFR sodium-cooled fast reactor
SRO short-range ordering
TO terminal oxygen
U.S. United States

U.S.S.R. Union of Soviet Socialist Republics

UV ultraviolet

WVDP West Valley Demonstration Project

ZIT zinc-in-titania

^a Formerly University of Missouri Rolla

1. INTRODUCTION

Glass is one of the most highly studied materials for immobilizing radioactive wastes. While borosilicate glasses are the most commonly studied glass-based waste form, phosphate glasses, the topic of this paper, are the second most important and studied glass waste form. A historical overview of phosphate glass waste form production along with specific milestones that lead to those decisions is provided in Table 1-1 (Park et al. 2008; Song et al. 2010; Siemer 2012; Vienna et al. 2015; Riley et al. 2020). Table 1-1 provides a general timeline that includes background information for borosilicate glass production milestones including research in the U.S. as well as other countries.

Phosphate glasses were first developed over 120 years ago for their high refractive indices, low chromatic dispersion, and high ultraviolet light transmission (in the case of alkaline earth phosphate glasses) compared to silicate glasses (Brow 2000; Kurkjian and Prindle 2005). Due to their unique optical, electrical, magnetic, mechanical, chemical, and thermal properties, phosphate glasses were investigated for different applications including photonics (Fletcher et al. 2011), batteries (Yamauchi et al. 2013), and biomedical materials (Ahmed 2019) in addition to nuclear waste forms (Brezneva et al. 1979; Sales and Boatner 1984b; Sales and Boatner 1984a; Day et al. 1998; Kim et al. 2003; Stefanovsky et al. 2015a; Stefanovsky et al. 2017; Stefanovsky et al. 2019). However, the low chemical durabilities of early phosphate glasses prompted the development of more chemically-durable glass formulations (Brow 2000).

Chemically durable iron phosphate glasses were eventually developed for the storage of nuclear waste forms using select glass-forming additives (Kim et al. 2003; Day and Ray 2013; Brow et al. 2019; Ebert and Fortner 2019; Riley and Chong 2020; Riley et al. 2020). The development of a phosphate glass system for immobilizing Hanford low-activity waste (LAW), which was generated from nuclear weapons production during World War II and the Cold War, was driven by a desire to increase loading of high-sulfur and high-sodium wastes in glass and thereby reduce the cost and schedule (Kim et al. 2003). It was pointed out that, although this technology was not fully developed in the U.S., the Mayak plant located in Chelyabinsk (Russia) had been producing aluminophosphate glasses to immobilize high-level nuclear waste (HLW) since the 1980s (Brezneva et al. 1979; Stefanovsky et al. 2015a; Stefanovsky et al. 2015b; Stefanovsky et al. 2017; Stefanovsky et al. 2019). Furthermore, it was found that the iron phosphate glass compositions could be successfully melted with little corrosion to alumina-zirconia-silicate (AZS), mullite, alumina, or Denver fireclay (DFC) ceramic refractory materials as well as little corrosion to Inconel 690 or molybdenum electrodes (Kim et al. 2003). These advances allowed for further development of the iron phosphate waste forms.

The basic goals of making successful radiological waste forms are that they will (1) withstand natural corrosion over geological time scales in a repository, (2) remain stable during this time under the decay of the radionuclides in the waste form, and (3) immobilize high quantities of radionuclides (i.e., have high waste loading). The goal of increasing the waste loading is to minimize the waste form volume thereby reducing the cost of fabrication, storage, transportation, and disposal.

The scope of the current paper is to provide an overview of what is known on the structure of phosphate glasses, relevant properties that pertain to nuclear waste forms (e.g., chemical durability and radiation stability). These are all things that were identified in a recent roadmap report (Riley et al. 2021) outlining technology gaps for advancing the use of phosphates to treat and immobilize salt-based waste streams. The structural properties of phosphate glasses are discussed including the different bonding environments that are created depending on the oxygen-to-phosphorus molar ratio in the glass, which leads to different amounts of bridging oxygens (BOs) and non-bridging oxygens (NBOs) and affects the chemical durability as well as other properties. Changing these parameters in phosphate glasses lead to glasses with a range of properties. Some of the more important properties from a waste form perspective include chemical durability, radiation stability, and the waste loading. Several other aspects are important such as the simplicity of the waste form production process, ease of process scale-up, phase distribution in the waste form following slow cooling (after melting and casting), and the cost of waste form production.

Table 1-1. Example of events regarding phosphate waste form development technologies.

Timeline	-1. Example of events regarding phosphate waste form development technolog Critical historical event (with references) ^(a)	Country ^(b)
1950's	Development begins on Na-Al-P-O glasses for Defense HLW	U.S.S.R.
1967–1970	Brookhaven National Laboratory develops phosphate glass for liquid metal fast breeder reactor (LMFBR)	U.S.
1960's–1970's	Phosphate marbles are developed in metal matrix in Karlsruhe for the Pilot Anlage Mol zur Erzeugung Lagerfähiger Abfälle (PAMELA) in Belgium	Germany
1966–1972	The Pacific Northwest Laboratory (PNL) develops phosphate glass for Waste Solidification Engineering Prototypes	U.S.
1978	The world's first full-scale HLW vitrification facility comes on-line in Marcoule producing borosilicate glass (BSG)	France
1979–1981	Hench Panel recommends BSG for US Defense HLW	U.S.
1982	Record of Decision for the Defense Waste Processing Facility (DWPF) (selecting BSG) (confirmed during National Environmental Policy Act in 1983)	U.S.
1982	West Valley Demonstration Project (WVDP) selects BSG as final waste form (preferred option following an Environmental Impact Statement)	U.S.
1984	WVDP analysis of alternative waste form options select BSG	U.S.
1977–1987	Alternative waste form options are evaluated for Hanford double-shell tanks (DSTs) including phosphate, BSG, ceramic WFs, and other options	U.S.
1984–1986	Oak Ridge National Laboratory develops lead iron phosphate glass with improved durability for US Defense HLW	U.S.
1987	First HLW Na-Al-P-O glass production at Mayak	U.S.S.R.
1987–1988	Record of Decision for Hanford DSTs, then all tank waste (selecting BSG for both)	U.S.
1990	Hanford reevaluates tank waste form selection, concurring with BSG selection	U.S.
1990's-present	Fe-P-O glasses evaluated by University of Missouri at Rolla (currently MUST) with lower tendency to devitrification and lower corrosion for various waste streams	U.S.
1995–1999	DOE Office of Materials Disposition (currently NA-233) evaluated forms for Pu immobilization including phosphate glass (they select Synroc)	U.S.
2008–2011	DOE Office of Environmental Management (DOE-EM) to develop next-generation melters and glass (include iron phosphate glass and cold crucible induction melting)	U.S.
2008-2010	Crystalline silica aluminophosphate (SAP) (Park et al. 2008) and zinc-in-titania (ZIT) (Song et al. 2010) waste forms developed for used ER salts	R.O.K.
2009–2012	MUST Nuclear Energy University Partnership (NEUP) on Fe-P-O glass corrosion	U.S.
2011	Siemer (Siemer 2012) (formerly from Idaho National Laboratory) evaluates Fe-P-O glass for Integral Fast Reactor (IFR) salt waste	U.S.
2012	DOE-EM decision not to further pursue next-generation melters and glass	U.S.
2013–2017	Mo-Sci Corporation initiates a Small Business Innovation Research contract on Fe-P-O nuclear waste glass development	U.S.
2015	DOE-NE defines baseline waste management technologies for advanced fuel cycle (focus on sodium-cooled fast reactor or SFR) (recommends BSG for aqueous HLW and ceramic waste form for electrochemical recycling salt for used nuclear fuel reprocessing) (Vienna et al. 2015)	U.S.
2017–present	DOE-NE develops Cl recycle flowsheet for echem salt with FeP glass (based on literature data) (Riley et al. 2020)	U.S.

(a)BSG = borosilicate glass, DST = double-shell tank, MUST = Missouri University of Science and Technology (formerly University of Missouri Rolla), SAP = silica aluminophosphate

(b)U.S.S.R. = Union of Soviet Socialist Republics, U.S. = United States, R.O.K. = Republic of Korea

2. PHOSPHATE GLASS STRUCTURE-PROPERTY RELATIONSHIPS

2.1 Short-Range Ordering in Phosphate Glasses

Phosphate glasses are composed of phosphate tetrahedron building blocks. The electron configuration of phosphorus is $[Ne]3s^23p^3$ and it has five valence electrons (Cotton and Wilkinson 1980). In the case of the phosphate (PO_4^{3-}) oxyanion where the phosphorus is covalently bonded to oxygen, the outer electrons are sp^3 hybridized with 4σ bonds and 1π bond with the oxygen 2p electrons (Cotton and Wilkinson 1980). In phosphate crystals, glasses, and melts, the nearest-neighbor phosphate tetrahedra link through BOs, although the π -bonded oxygen does not participate in bonding and is often observed to be significantly shorter than the other three (Cotton and Wilkinson 1980). The degree of tetrahedral linking in a glass is classified using "Q"" notation where n = 0-3, representing the number of BOs per tetrahedron, and the quantity 3-n represents the number of NBOs (see Figure 2-1). Since these provide a description of the first-and second-coordination spheres around the phosphorus atoms, we can consider this as the short-range ordering (SRO) of phosphate glass backbone.

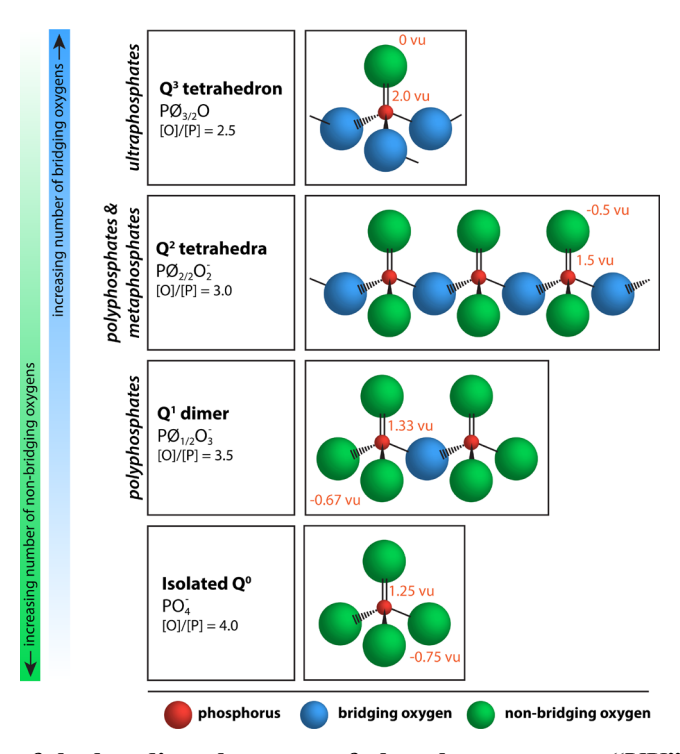


Figure 2-1. Description of the bonding character of phosphate systems. "VU" denotes valence units.

In phosphate glass systems the degree of tetrahedral linking has been observed in the range of Q^3 (a cross-linked network, referred to informally as vitreous P_2O_5), to Q^2 (a polymer-like metaphosphate), Q^1 (small pyrophosphate dimers), and Q^0 (isolated orthophosphate islands) as shown in Figure 2-1. The molar ratio of the oxygen-to-phosphorus (i.e., [O]/[P]) in the glass system largely determine the distribution of the Q-species in the glass. Spectroscopic measurements, such as ^{31}P magic angle spinning nuclear magnetic resonance (i.e., ^{31}P MAS NMR), can be utilized to quantify the relative fractions of the Q^n units, see Figure 2-2 (Brow et al. 1994; Brow et al. 1995). It should be noted that in MAS NMR techniques, the chemical shift (in units of ppm) is relative to a standard material (e.g., 85% H₃PO₄ solution) and the peak position is observed to vary slightly due to matrix effects and measurement parameters.

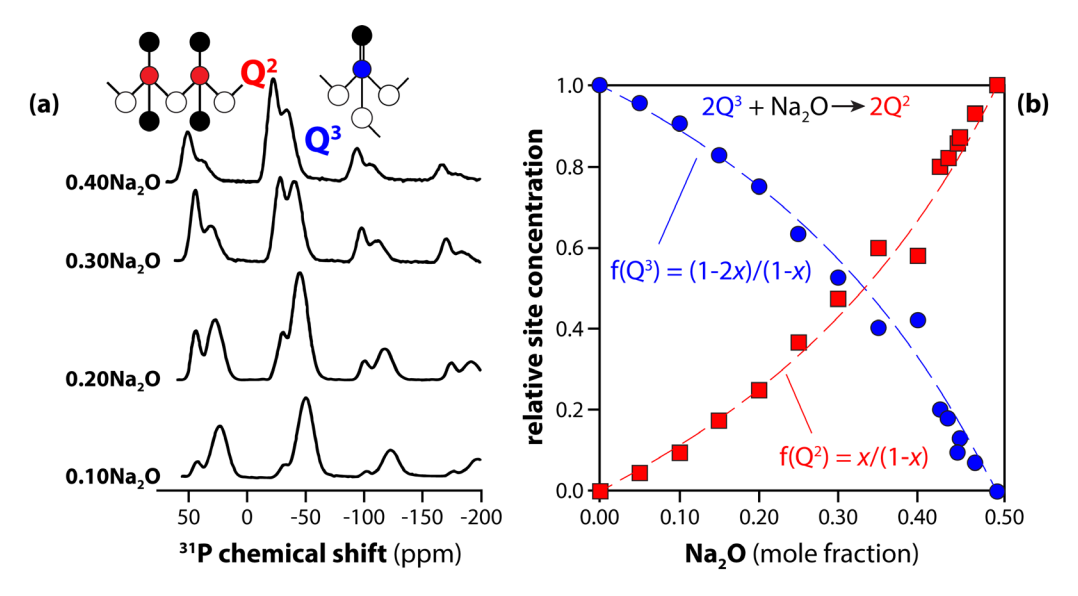


Figure 2-2. (a) ³¹P MAS NMR of xNa₂O-(1-x)P₂O₅ glasses with varying additions of Na₂O demonstrating the spectroscopic signatures of Q² and Q³ species at -20 and -51 ppm and (b) the quantified fraction of Q² and Q³ species, denoted as f(Q"), as a function of Na₂O addition with lines provided to guide the eye. This figure was modified from the original (Brow et al. 1994).

2.2 Medium-Range Ordering in Phosphate Glasses

Beyond the first- and second-coordination spheres that makeup the SRO of the phosphorus atoms, there exists ordering in the glass networks at longer length scales, which is referred to as the medium-range ordering (MRO). Both of these ordering scales are much shorter than what is exhibited by crystalline materials with long-range ordering (LRO). Detailed structural understanding of vitreous P_2O_5 has only been gained recently because vitreous P_2O_5 is hygroscopic and volatile, requiring the use of a dry glovebox for chemical storage and glass synthesis (Brow 2000). The total distribution function obtained through neutron scattering revealed two coordination signatures corresponding to 3 bonding oxygens (BO) and one π -bonded terminal oxygen (TO) per tetrahedral unit, which makeup the description for the SRO of vitreous- P_2O_5 (Brow 2000). The MRO was also understood using neutron total scattering, in this case the structure factor [i.e., S(Q)] was used. The neutron S(Q) is the coherent scattering term in the differential neutron scattering cross-section (Keen 2001). The first and second diffraction peaks in the S(Q) correspond to an average periodicity in the glass systems of 4.8 and 3.0 Å, respectively, which are comparable to the intermolecular distances found in a polymorph of crystalline P_2O_5 (Brow 2000). The details on the nature and the extent of the ordering are still under investigation.

In Figure 2-2 and Figure 2-3, binary glass compositions were utilized where vitreous- P_2O_5 is systematically mixed with $(R^+)_2O$ or $(R^{2+})O$, where R^+ is a monovalent network modifier (e.g., Na^+) and R^{2+} is a divalent network modifier (e.g., Ca^{2+}), both of which break-up the network of vitreous- P_2O_5 (Brow et al. 1994; Brow et al. 1995; Brow 2000). The properties of these glasses vary with the amount of added network-modifying species (i.e., x) where the binary glass composition can be written as $x(R^+)_2O \cdot (1-x)P_2O_5$ or $x(R^{2+})O \cdot (1-x)P_2O_5$ depending on the additive. Phosphate glasses have been defined in three main categories depending on x, the fraction of $(R^+)_2O$ or $(R^{2+})O$ (Brow 2000) including ultraphosphates, metaphosphates, and polyphosphates. *Ultraphosphate* glasses exist in the compositional regime of $0 \le x \le 0.5$ and are comprised of Q^2 and Q^3 tetrahedral units. *Metaphosphate* glasses exist at x = 0.5 and are primarily comprised of Q^2 units in chains or rings connected by the ionic bonds between NBO and the metal cations $(R^+)_2O \cdot (R^2)_2O \cdot$

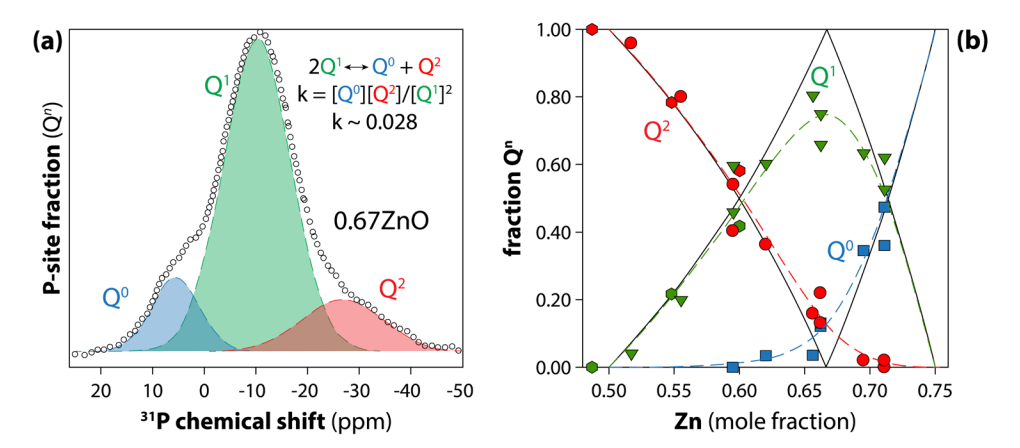


Figure 2-3. (a) ³¹P MAS NMR of xZnO-(1-x)P₂O₅ glass demonstrating the spectroscopic signatures of Q⁰, Q¹, and Q² species at +5.6, -10.7, and -28.6 ppm, respectively. (b) the quantified fraction of Q⁰, Q¹, and Q² species as a function of ZnO addition with lines provided to guide the eye. These figures were modified from the originals (Brow et al. 1995; Sales et al. 1998; Brow 2000).

In polyphosphate glasses, the length of the constituent chains are shorter as the ratio of [O]/[P] increases; this is shown in Figure 2-4 (Brow 2000). For phosphate glasses the following structure-compositions exist (Brow 2000) where [O]/[P] = 3.125 leads to an average chain length of 8 (6Q² and 2Q¹), [O]/[P] = 3.25 leads to an average chain length of 4 (2Q² and 2Q¹), [O]/[P] = 3.5 is the stoichiometric ratio for polyphosphate and the average chain length is 2 (dimers of Q¹ tetrahedra), and [O]/[P] > 3.5 is where glasses contain isolated Q⁰ units, referred to as 'orthophosphate' units.

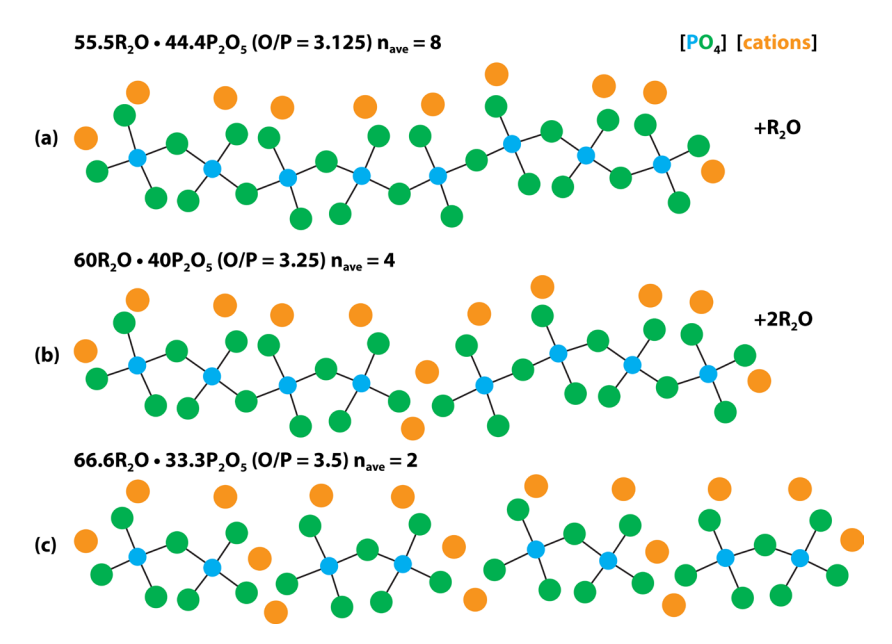


Figure 2-4. Schematic representation of the influence of composition on the MRO in xR_2O -(1-x) P_2O_5 polyphosphate glass through the decrease in average chain length (n_{avg}) as a function of x. This figure was modified from the original (Brow 2000).

As the chain length varies in polyphosphate glasses as a function of [O]/[P], the number of NBOs increases, therefore the average charge per chain (referred to as the 'NBO charge') increases, as summarized in Figure 2-5a. This interplay between chain length and electrochemical properties influences the properties of the glass including the chemical durability. Chemical durability in iron-phosphate glasses is also affected by

the [Fe]/[P] ratio, which is shown in Figure 2-5b and Figure 2-5c. In the regime of x > 0.6, in the so-called "modifier-rich" phosphate glasses, the glass network is a continuous network of metal-oxygen polyhedra that are linked through phosphate units (i.e., predominantly Q^0 , Q^1 , and Q^2) (Onodera et al. 2017).

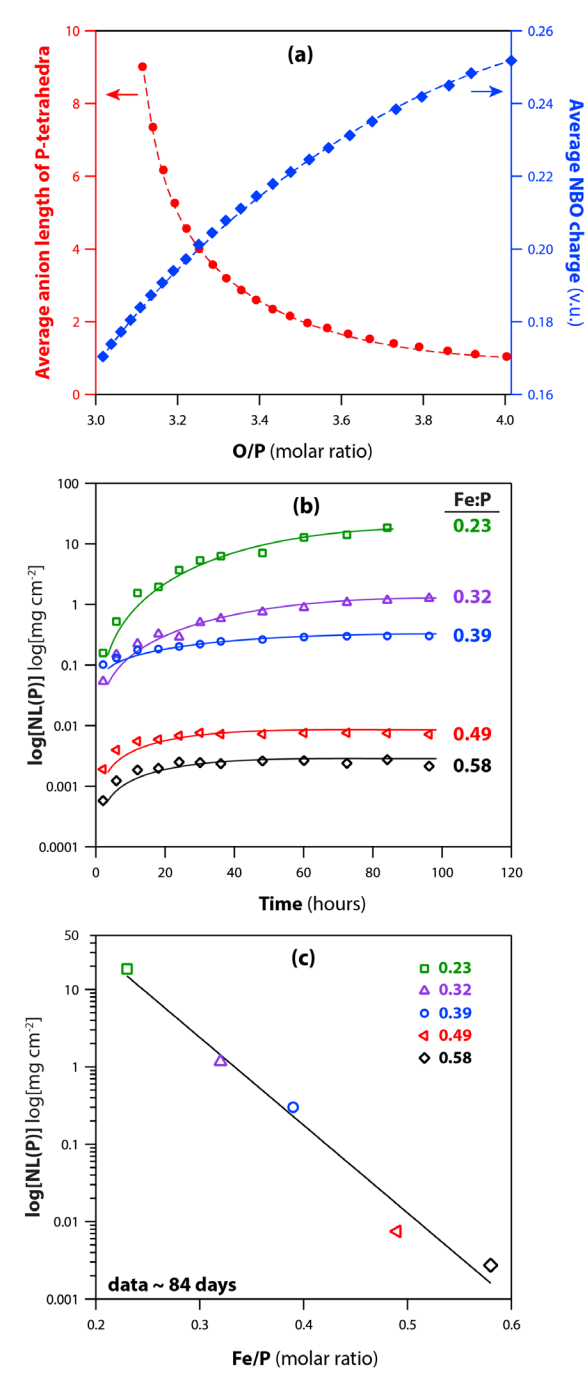


Figure 2-5. (a) Effect of the [O]/[P] ratio on the average PO_4 -anion chain length in polyphosphate glasses (see Figure 2-4) and the average charge per chain due to the presence of terminal NBO. (b) Summary of iron phosphate glass dissolution rate as a function of time for different Fe:P molar ratios at a fixed [O]/[P] of 3.40±0.03 and (c) the semilog plot of log[NL(P)] vs the Fe:P molar ratio (Ma et al. 2017).

The distribution of the chain lengths of polyphosphate glasses is experimentally determined using chromatographic analysis of solutions prepared through the leaching of glasses (Brow 2000). High-pressure liquid chromatography (HPLC) was performed in previous work by Ma et al. (Ma and Brow 2014; Ma et al. 2018) to characterize the size of the phosphate chain anions by crushing 200 mg of glass powders to a particle size distribution of 75–150 μ m and partially dissolving for different time lengths ranging from 2–12 hr in a 0.22 M NaCl solution with 5mM sodium ethylenediaminetetraacetic acid (EDTA) at a pH of 10; the EDTA was added as a chelating agent to prevent hydrolysis of the dissolved phosphate anions. Figure 2-6 shows HPLC chromatographs of sodium-calcium polyphosphate glasses as a function of [O]/[P] ratio and peaks are denoted with P_n where n is associated with specific phosphate anions comprised of nPO4 tetrahedra (Ma et al. 2018). The integrated peak area is proportional to the relative concentration of the $(P_nO_{3n+1})^{(n+2)-}$ phosphate anions (Ma et al. 2018). However, for phosphate anions with n > 12 these species are not resolvable. Lastly, the number of Q^3 sites, which can be found in ultraphosphate glasses, cannot be determined through HPLC methods as they readily hydrolyze.

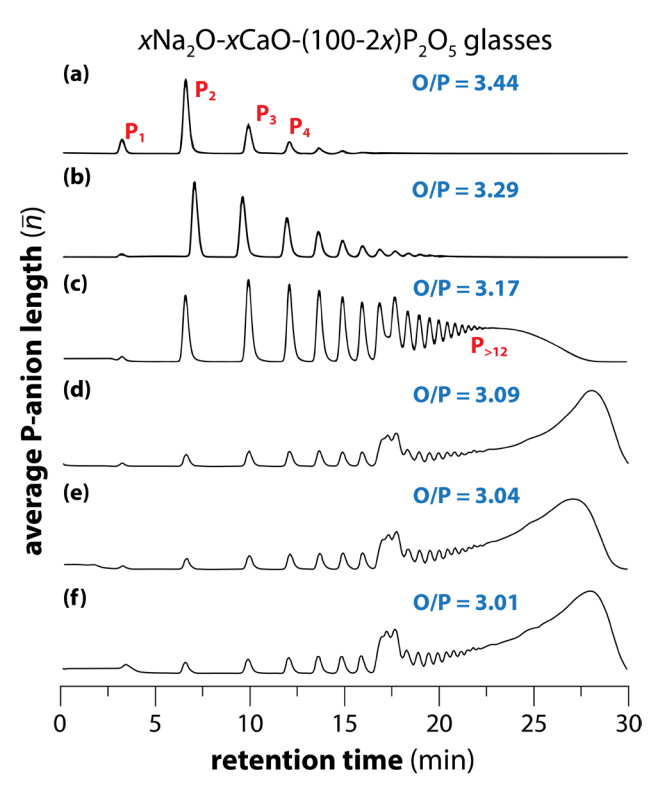


Figure 2-6. HPLC chromatographs for $xNa_2O \cdot xCaO \cdot (1-2x)P_2O_5$ polyphosphate glasses where the [O]/[P] ratio was (a) 3.44, (b) 3.29, (c) 3.17, (d) 3.09, (e) 3.04, or (f) 3.01. The chain lengths are provided next to the relevant peaks. This figure was modified from the original (Ma et al. 2018).

2.3 Iron Phosphate Glasses for Nuclear Waste Remediation

The addition of less than 10 mol% Fe_2O_3 to sodium-calcium phosphate glasses can significantly increase the chemical durability in aqueous media (Brow et al. 2019). In one study, 5 mol% Fe_2O_3 reduced the aqueous degradation of $20Na_2O\cdot30CaO\cdot50P_2O_5$ glass by nearly two orders of magnitude (Brow et al. 2019). In another study, 15 mass% HLW was loaded into a lead iron phosphate glass and subjected to 30-day 90°C static corrosion tests as a function of pH (Sales and Boatner 1984b). The resulting corrosion rates were found to be comparable or lower than a borosilicate glass with a similar waste loading (Sales and Boatner 1984b).

A study by Day et al. (1998) shows that some of the Hanford HLW contains up to 15 mass% P₂O₅, up to 25 mass% Fe₂O₃, up to 30 mass% heavy metal oxides (e.g., Bi₂O₃), and up to 30 mass% UO₂. The presence of such high levels of P₂O₅ and heavy metals raises concern of the possibility of phase separation or liquid immiscibility if added to a borosilicate matrix, which could significantly affect the chemical durability of these waste forms (Day et al. 1998). In order to incorporate such high fractions of P₂O₅ and heavy metals into a borosilicate glass without inducing phase separation or similar deleterious effects, the waste would have to be treated or diluted, which would increase the final volume of the waste form (Day et al. 1998). By using an iron phosphate glass where the [O]/[P] was in the range of 3.46–4.43, it was hypothesized that the waste form volume could be reduced by 20–33 vol% while still meeting the necessary processing parameters and chemical durability requirements for borosilicate glasses (Day et al. 1998; Perez et al. 2001). The liquidus surface for the ferric phosphate system is shown in Figure 2-7, with an annotation showing the commonly-studied glass-forming region corresponding to [O]/[P] ratios near 3.5 (Brow et al. 2019) (also shown in Figure 2-8 (Day and Ray 2013)). Most available studies have focused on polyphosphate compositions in the range of 25 Fe₂O₃-75 P₂O₅ to 50Fe₂O₃-50P₂O₅ (corresponding to [Fe]/[P] of 0.33–1.00 and [O]/[P] of 3–4, respectively) (Brow et al. 2019).

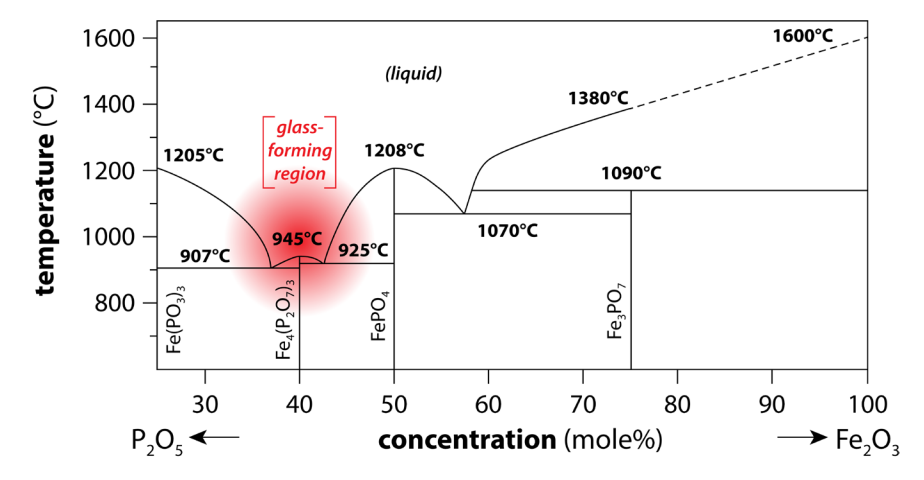


Figure 2-7. (top) Liquidus surface for the $Fe(PO_3)_3 \cdot Fe_2O_3$ system exhibiting the glass-forming range of interest nuclear waste iron phosphate glasses (Brow et al. 2019). (bottom) Liquidus surface for the $Fe(PO_3)_3 \cdot Fe_4(P_2O_7)_3$ compositional range which of interest for nuclear waste immobilization.

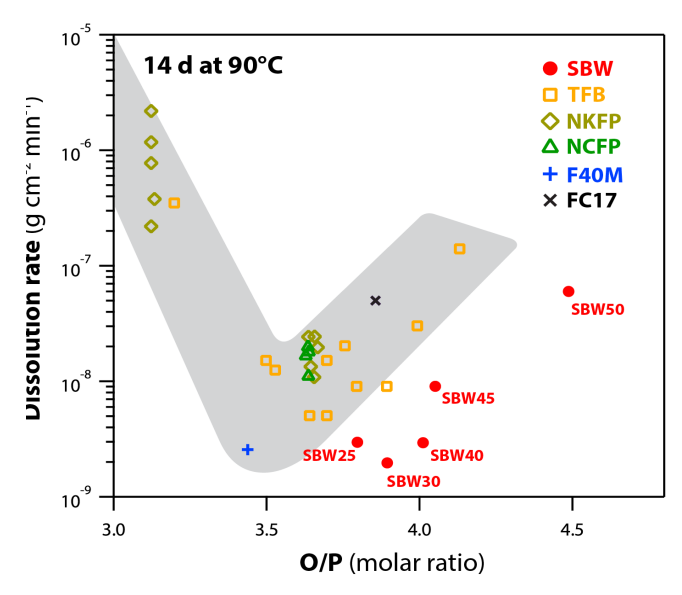


Figure 2-8. Compiled dissolution rates for phosphate glasses mixed with various simulated waste compositions as a function of [O]/[P] ratio. This figure was modified from the original by Day et al. (Day and Ray 2013).

Although iron phosphate glasses are binary glasses since they only contain Fe and P cations, these glasses are better described as FeO·Fe₂O₃·P₂O₅ glasses since they likely contain both ferrous (Fe²⁺) and ferric (Fe³⁺) ions depending on selected synthesis reagents and the processing conditions used during processing and melting (Brow et al. 2019). Both iron oxidation states can assume different coordination numbers with oxygen, i.e., tetrahedral (4-coordinated) or octahedral (6-coordinated), which in turn affects local bonding environments within the glass network. Experimentally, the fractions of ferrous and ferric species can be determined using Mössbauer spectroscopy, wet-chemical methods, or X-ray absorption techniques (Magnien et al. 2006). For 40Fe₂O₃·60P₂O₅ glass with a fraction of reduced iron Fe²⁺/(Fe_{tot}) = 0.2–0.4 [see Equation (1); Fe_{tot} = total iron], both Fe²⁺ and Fe³⁺ ions were found in octahedrally coordinated (bonded to 6 oxygens) environments that linked diphosphate anions (dimers of P₂O₇⁴⁻) (Brow et al. 2019) as are shown schematically in Figure 2-9.

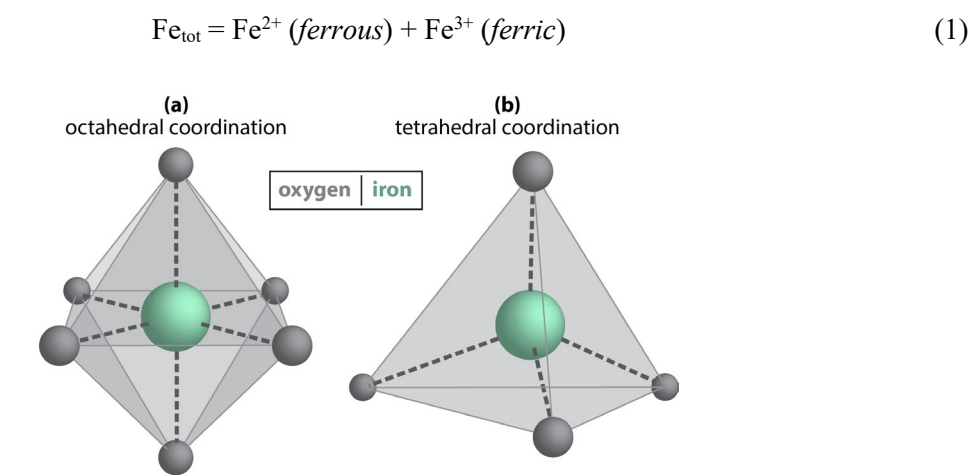


Figure 2-9. Graphical representations of (a) octahedral coordination and (b) tetrahedral coordination environments commonly found for Fe²⁺/Fe³⁺.

Another aspect of glass composition to consider is the choice of the source chemicals during batching. For instance, the choice of phosphate precursor(s) [e.g., P₂O₅, H₃PO₄, NH₄H₂PO₄, (NH₄)₂HPO₄] used during phosphate glass synthesis can affect the properties of the melt as well as the final glass. Regarding the melt, if H₃PO₄, NH₄H₂PO₄, or (NH₄)₂HPO₄ are used, volatile off-gas products (e.g., H₂O, NH₃) will be evolved that can lead to splattering or bubbling of the melt onto the melting vessel. Figure 2-10 shows the impact on Fe²⁺ and Fe³⁺ in the glass when using H₃PO₄ vs NH₄H₂PO₄, where H₃PO₄ results in a more oxidized glass (i.e., $Fe^{2+}/Fe_{tot} = 5$ mass%) than when $NH_4H_2PO_4$ was used (i.e., $Fe^{2+}/Fe_{tot} = 53$ mass%) (Bai et al. 2020). Figure 2-10 provides Mössbauer spectra of 15Cs₂O·yMoO₃·(28.75–y)Fe₂O₃·56.25P₂O₅ glasses prepared with H₃PO₄ or NH₄H₂PO₄ phosphorus sources. In the glass made with H₃PO₄, the iron was found to be present in nearly equal fractions of octahedral and tetrahedral coordination with oxygen (<5% was found to be octahedrally-coordinated Fe²⁺) (Brow et al. 2019). In the sample made with NH₄H₂PO₄, the significantly higher fraction of reduced Fe²⁺ was found as octahedrally coordinated species. The fraction of ferrous iron acts to reduce the physical properties of the glass, for example, by decreasing the kinetic parameter, which describes the fictive temperature induced into the glass-forming melt upon cooling. The goal of pushing for a higher Fe³⁺/Fe²⁺ ratio in the final product is that the oxidized glasses can have higher chemical durability as demonstrated in the study by Yu et al. (1997) on sodium iron phosphate glasses.

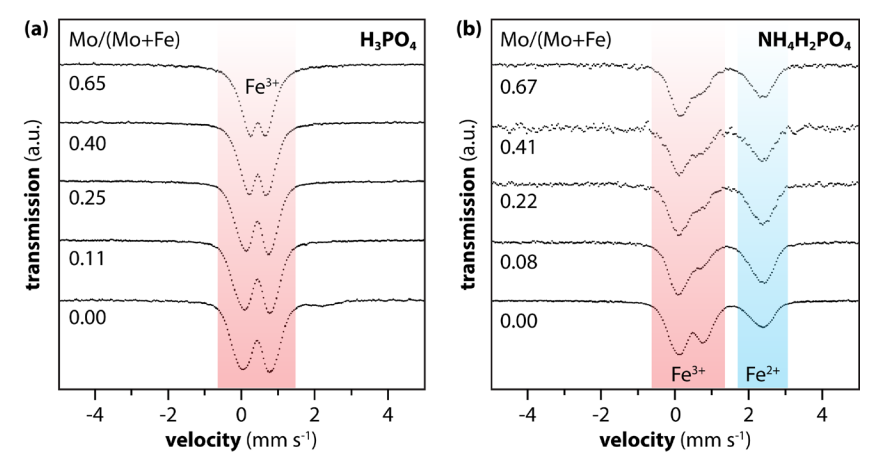


Figure 2-10. Summary of Mössbauer spectroscopy of $15Cs_2O \cdot yMoO_3 \cdot (28.75 - y)Fe_2O_3 \cdot 56.25P_2O_5$ glasses showing Fe²⁺ and Fe³⁺ in glasses with similar targeted composition batched with either (a) H₃PO₄ or (b) NH₄H₂PO₄. The regions representing Fe²⁺ and Fe³⁺ species are labeled accordingly. The Fe²⁺ concentration (from total Fe, i.e., Fe²⁺ + Fe³⁺) measured in (a) and (b) were 5 mass% and 53 mass%, respectively. This figure was modified from the original (Bai et al. 2020).

The HPLC results of iron-bearing polyphosphate glasses in Figure 2-11a–Figure 2-11c, show a similar trend as that shown in Figure 2-6 for polyphosphate glasses where the sizes, n, of phosphate anions $(P_nO_{3n+1})^{(n+2)}$ decreases with increasing [O]/[P] (Ma and Brow 2014). Figure 2-11d provides a schematic of the general structure of sodium iron phosphate glasses (Ma and Brow 2014). In general, the addition of metal oxides into metaphosphate glasses increases the [O]/[P] ratio resulting in NBOs in the form of Fe–O–P and Na–O–P, which interrupt the P–O–P bonded network (Ma and Brow 2014). The schematic representation in Figure 2-11d demonstrates that in a prototypical iron polyphosphate glass, ferric and ferrous ions form polyhedra with the NBOs of the Q^1 and Q^2 units present in the polyphosphate chain anions similar to alkali and alkaline earth cations (Bingham and Barney 2012; Brow et al. 2019). Some controversy still exists regarding the precise structural aspects of phosphate glasses that provide these systems with their macroscale properties (Wright et al. 2008; Bingham and Barney 2012).

11

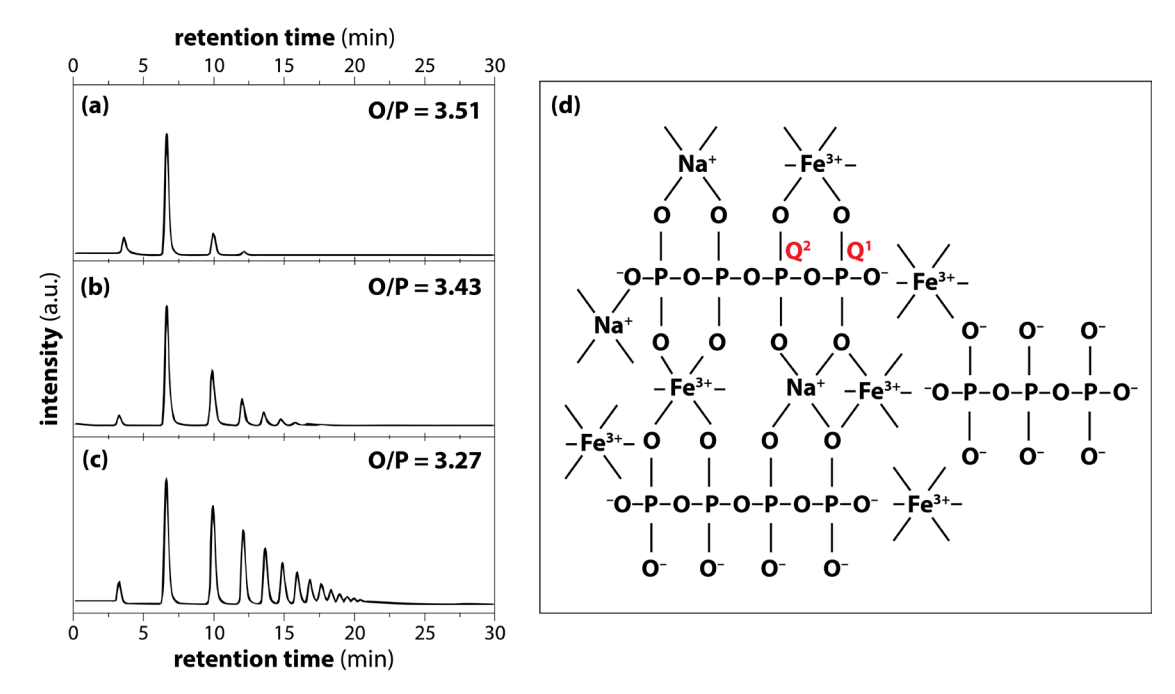


Figure 2-11. (a-c) HPLC of sodium-iron phosphate glasses with different [O]/[P] ratios of (a) 3.51, (b) 3.43, and (c) 3.27. (d) Schematic of the general structure of sodium iron phosphate glasses. This figure was modified from the original by Ma and Brow (2014).

2.4 Dissolution Behavior of Phosphate Glasses

Vitreous P_2O_5 , $R_2O-P_2O_5$ glasses, and glasses composed of $(R^+)_2O\cdot(R^{2+})O\cdot P_2O_5$ (e.g., $Na_2O\cdot CaO\cdot P_2O_5$) are known to have low chemical durabilities in aqueous environments (Brow 2000; Riley et al. 2020). However, the addition of 5 mol% Fe_2O_3 reduced the aqueous degradation of $20Na_2O\cdot 30CaO\cdot 50P_2O_5$ glass by nearly two orders of magnitude (Brow et al. 2019). Figure 2-8 shows that the lowest dissolution rates were observed in the [O]/[P] of 3.4–4.0, depending on the compositions of the waste (Day et al. 1998; Day and Ray 2013). Most of the dissolution rates observed for the waste glasses made based on the Hanford Tank Farm B waste stream were in the range of 3×10^{-9} to 3×10^{-7} g cm⁻² min⁻¹ (i.e., $\sim 4\times 10^{-2}-4\times 10^{0}$ g m⁻² d⁻¹) (Day et al. 1998) for bulk samples $(1\times 1\times 0.1 \text{ cm}^3 \text{ in } 100 \text{ mL DIW for } 14 \text{ days at } 90^{\circ}\text{C})$ exposed to 90°C DIW. For comparison, the dissolution rates of two borosilicate waste glasses, CVS-IS and LD6-54-12, in 90°C deionized water for 14 days were 2.6×10^{-8} and 8.8×10^{-9} g cm⁻² min⁻¹ (i.e., $\sim 3.7\times 10^{-1}$ and $\sim 1.3\times 10^{-1}$ g m⁻² d⁻¹, respectively) using the same conditions $(1\times 1\times 0.1 \text{ cm}^3 \text{ in } 100 \text{ mL DIW for } 14 \text{ days at } 90^{\circ}\text{C})$ (Day et al. 1998).

Based on the structural influence of the [O]/[P] ratio on the size of the polyphosphate anions, it was determined that the normalized release [i.e., NL(i) for element i] was less for glasses with higher [O]/[P] ratios (i.e., shorter P_nO_{3n+1} chains) as shown in Figure 2-12 (Ma et al. 2018). Fundamentally, the shorter chains feature fewer Q^2 units and have more NBO per tetrahedral unit therefore have stronger metal–NBO bonds and pack into more denser structures (Ma et al. 2018). As will be described later in this section, the release of phosphorus anions from polyphosphate glasses is driven by the breakage of metal–O–P bonds (Ma et al. 2017).

The releases of Na, P, and Ca species in $xNa_2O \cdot xCaO \cdot (1-2x)P_2O_5$ glasses were mostly congruent as shown in Figure 2-12a (Ma et al. 2018). Figure 2-12 demonstrates that when sodium calcium phosphate glasses are placed in an aqueous environment, the pH changes as a function of time and [O]/[P] ratio (Ma et al. 2018). This is due to the addition of Na₂O and CaO to increase the [O]/[P] molar ratio (Ma et al. 2018). The Na₂O and CaO hydrolyze when leached and increase the pH of the leachate, whereas the hydrolysis of the P_nO_{3n+1} chains decreases the pH of the solution depending on the relative fraction of P_2O_5 (Ma et al. 2018).

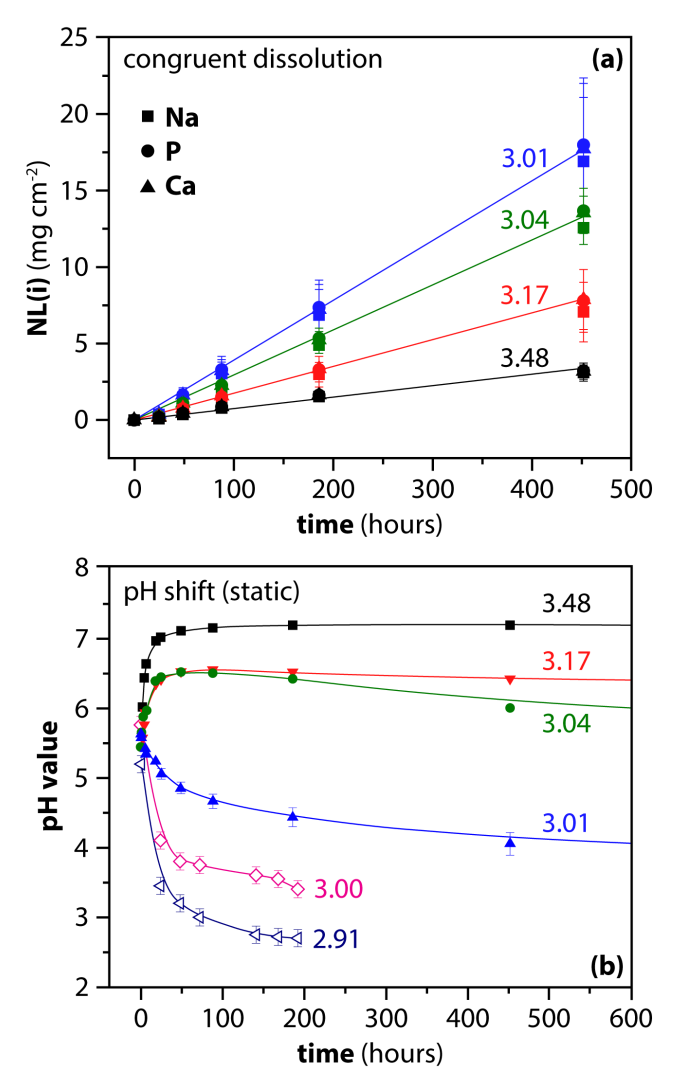


Figure 2-12. (a) normalized mass release (mg/cm²) values for sodium, calcium, and phosphorus and (b) pH of the leachate solutions for static dissolution of xNa₂O·xCaO·(1-2x)P₂O₅ glasses at room temperature as functions of time and [O]/[P] molar ratios, which are shown as the numbers on all datasets in (a) and (b). These figures were modified from the originals by Ma et al. (2018).

In general, the mechanism for glass dissolution is determined by the reactions of the glass network and the release of ions into the solution into which the sample is submersed (Vienna et al. 2013; Ma et al. 2017) (see Figure 2-13). The stages of dissolution can follow three main stages (Gin et al. 2013) as shown in Figure 2-13a. An initially fast rate (Stage-I) is initiated by interdiffusion of water into the glass structure, hydrolysis, and transport affinity phenomena. The ion exchange or diffusion of water molecules into the glass network leads to surface swelling see Figure 2-13b (Ma et al. 2017). Hydration of the phosphate ions breaks the (Na,Fe)–O–P bonds that link neighboring (P_nO_{3n+1})⁽ⁿ⁺²⁾⁻ anions leading to the release the anions and metal cations into solution (Ma et al. 2017). These initial stages of glass dissolution are followed up by a residual rate where the corrosion rate slows down (Stage-II). Then, for some glasses, the alteration renewal can sometimes take place after Stage-II (Stage-III).

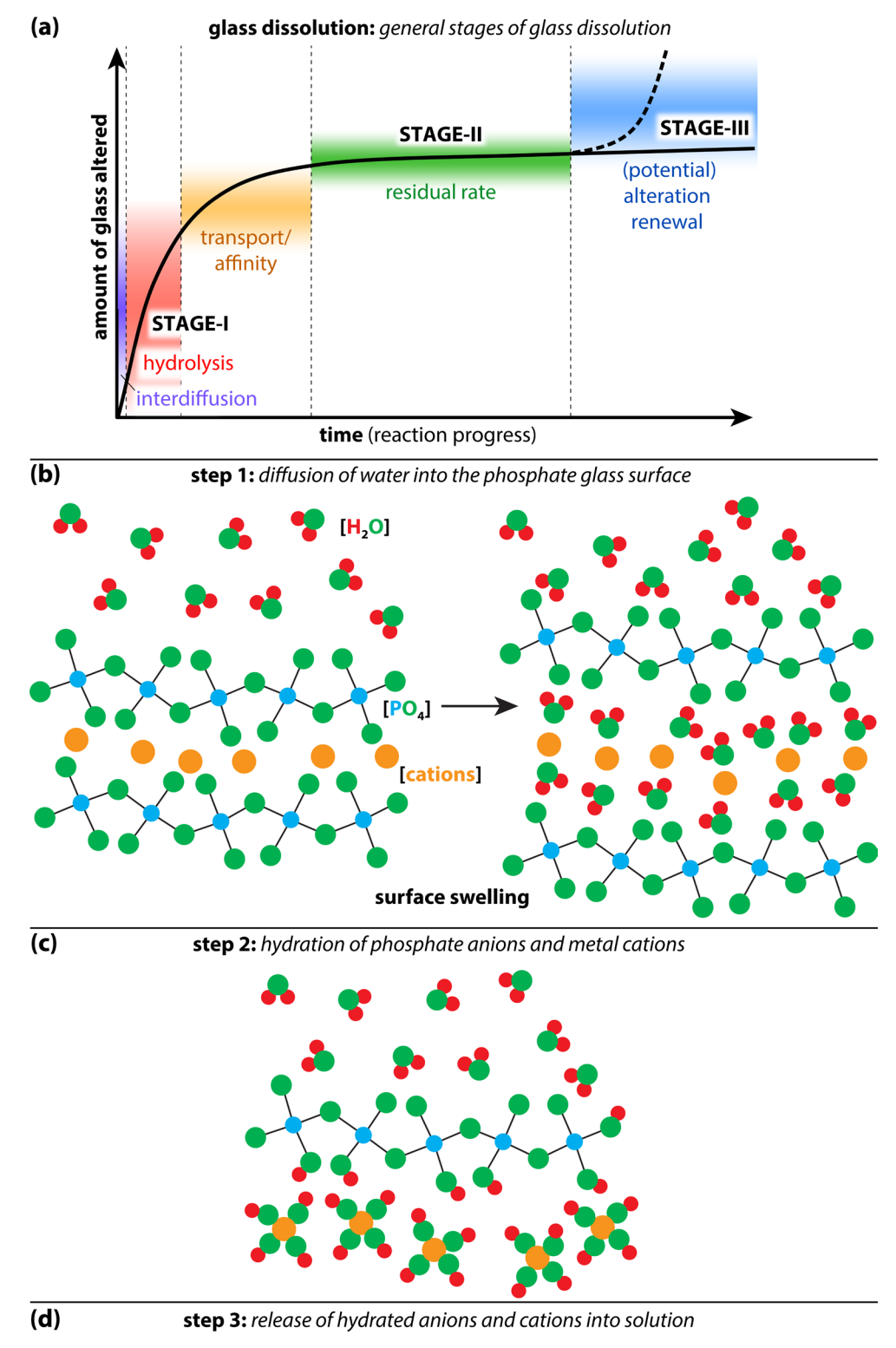


Figure 2-13. (a) General processes for glass dissolution [modified from the original by Vienna et al. (2013)]. (b-d) Schematic representation of the mechanism for the ingress of water into phosphate glasses and the subsequent leaching of hydrated ions into solution.

March 19, 2024

As described above, the dissolution of polyphosphate glasses is congruent for all atoms and is affected by the ratio of [O]/[P] in polyphosphate glasses, which also affects the length of the phosphorus ions (Brow et al. 1995; Lim et al. 2011; Ma et al. 2017). The increased chemical durability when iron is added to polyphosphate glasses can be observed as a function of the [Fe]/[P] ratio in Figure 2-14 where, at higher [Fe]/[P] ratios, incongruent dissolution is observed more with preferential release of elements in the order of Na > P > Fe (Ma et al. 2017).

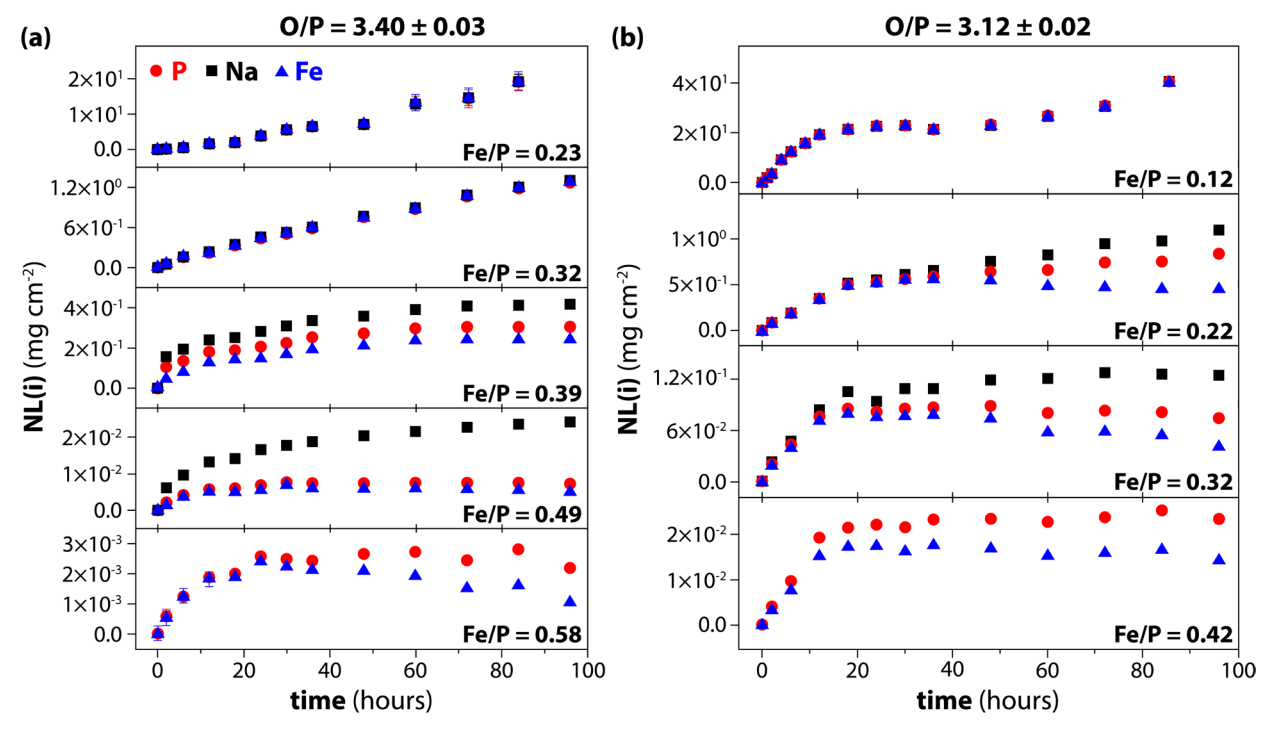


Figure 2-14. Normalized mass release of P, Na, and Fe as a function of time for glasses with (a) [O]/[P] = 3.4 and (b) with [O]/[P] = 3.12. This figure was modified from the original by Ma et al. (2017).

During dissolution tests, the fraction of dissolved phosphorus from the parent glass [i.e., $\alpha(P)$] increased as a function of time where static methods showed a smaller dependence on the [O]/[P] ratio than semidynamic tests (Ma et al. 2017; Ma et al. 2018). The dissolved fraction shows a clear transition from a square root time dependence ($\propto k_1 t^{1/2}$, where k_i is a rate parameter for the *i*-th process and t is time) to a linear time dependence ($\propto k_2 t$) (see Figure 2-15a) (Ma et al. 2017; Ma et al. 2018). Different shrinking core models were used to fit to the glass dissolution data wherein the glass particles used for corrosion tests were assumed to have spherical geometries that were dissolved isotropically by the surrounding solutions (Ma et al. 2017). A 3-dimensional diffusion model (DM) in Equation (2) was used to describe the square root time dependence and a contracting volume model (CVM) in Equation (3) was used to describe the linear time dependence (Ma et al. 2017) where α is the mass fraction of a particle reacted in time t.

$$1 - (1 - \alpha)^{1/3} = k_1 t^{1/2} \tag{2}$$

$$1 - (1 - \alpha)^{1/3} = k_2 t \tag{3}$$

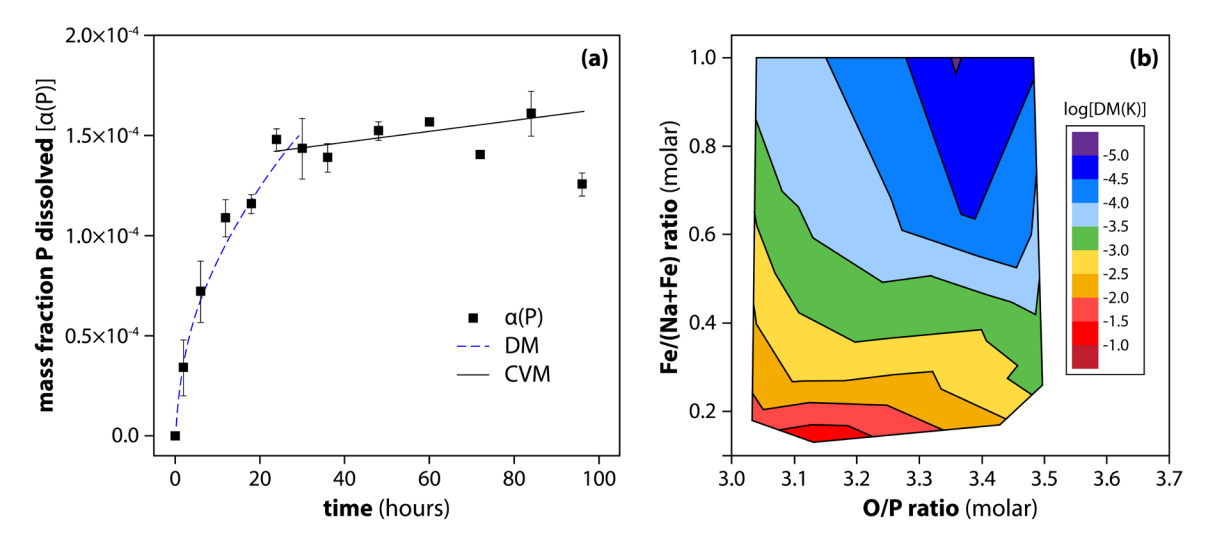


Figure 2-15. (a) Mass fraction of dissolved phosphorus $[\alpha(P)]$ as a function of time with two fit lines provided for DM (3D diffusion domain, proportional to $t^{1/2}$) and CVM (contracting volume domain, proportional to t). (b) Isosurface plot showing the compositional dependence of the rate parameter for the 3D diffusion model (k_1). These figures were modified from the original (Ma et al. 2017).

The reaction time where the DM domain transitioned to the CVM domain changed depending on the glass composition (Ma et al. 2017). Iron polyphosphate glasses with longer (P_nO_{3n+1}) chains and lower [O]/[P] ratios did not exhibit a significant change in the transition time as the [Fe]/[P] ratio increased in contrast to those glasses with shorter P_nO_{3n+1} chains where the transition occurred at prolonged times as the [Fe]/[P] ratio increased (Ma et al. 2017). Both k_1 and k_2 rate parameters show a dependence on the [Fe]/[P] ratio with the graph of k_1 provided in Figure 2-15a, demonstrating that with increased iron content iron polyphosphate glasses react more slowly in both the DM and CVM domains (Ma et al. 2017). Furthermore, the influence of the [Fe]/[P] ratio has a greater effect on the dissolution of iron polyphosphate glasses than the [O]/[P] ratio (Ma et al. 2017).

3. RADIATION TOLERANCE

The principal sources of radiation in HLW are β -decay of the fission products (e.g., ¹³⁷Cs and ⁹⁰Sr) and α -decay of the actinide elements (e.g., U, Np, Pu, Am, and Cm), both of which lead to physical and chemical changes in the waste form. Both α and β decay affect the structure of waste glasses through the interactions of the α particles, β particles, recoil nuclei, and γ rays with the glass. These interactions fall into two broad categories of (1) the transfer of energy to electrons including ionization and electronic excitations and (2) the transfer of energy to atomic nuclei, primarily by ballistic processes involving elastic (billiard-ball-like) collisions. For β particles and γ radiation, the energy transfer is dominated by ionization processes. For α particles and recoil nuclei, most of the energy will be transferred to the nucleus of the ions in their path.

Radiation effect studies on phosphate glasses were often done for photonic applications with relatively fewer studies being reported for waste form applications so more work is needed to better elucidate the effects of thermal and radiological stability for phosphate glasses (Heng et al. 2015; Dube and Hyatt 2019; Dube et al. 2020; Petit 2020b). For applications in nuclear waste forms, understanding the interaction between decaying fission products and the surrounding matrix of the waste form is crucial. The forms of ionization radiation including α particles, β particles, X-rays, and γ rays are emitted within the waste forms during decay of fission products, and their effects on the physical and chemical properties of waste forms need to be investigated thoroughly to develop robust and chemically durable waste forms.

The high waste loadings and high fission product loadings that can be achieved in iron phosphate waste forms will result in high decay heats being generated by fission products within the waste form. This will affect the stability of the waste form itself and heat transferred to the storage and disposal facilities. These evaluations should be considered for a variety of different possible waste streams. One of the primary issues that decay heat introduces into the qualification of a glass waste form is that, if the decay heat prohibits the waste form from rapidly cooling through critical phase transition temperatures (e.g., the glass transition temperature or T_g), this can lead to unwanted crystallization and, potentially, a lower chemical durability than that of the quenched glass. Heat loading calculations also take several other material properties into consideration such as the thermal diffusivity (α ; defined in Equation (4)], thermal conductivity (k), specific heat capacity (c_p), and density (ρ), all of which will depend on the base glass formulations, waste composition, and waste loadings. These intrinsic properties affect the rate at which decay heat can be transferred out of the waste form into the waste package and dissipated into the repository environment. In most engineered disposal facilities, the use of bentonite backfill material will impose thermal limits on disposed waste.

$$\alpha = k/(\rho \cdot c_p) \tag{4}$$

Radiation damage in a waste from can be manifested through the occurrence of several things including relaxation processes, diffusion processes, phase separation, devitrification, amorphization of crystalline phases, volume changes, cracking, gas accumulation, bubble formation, and/or void formation. The most important issue requiring more in-depth studies is the need for an understanding of the radiation-induced structural changes at the atomic, microscopic, and macroscopic levels, and the effects of these changes on the release rates of radionuclides during corrosion. Specifically, very few studies have been done to evaluate the radiation-induced formation of defects and microscopic evolution in phosphate glasses and none of these studies have been directed at the types of compositions to be expected from treating or immobilizing salt streams from electrochemical reprocessing or molten salt reactors, for example.

3.1 Radiation-Induced Defects

Radiation-induced defects in phosphate glasses include phosphorous-oxygen hole centers (POHC), phosphorus-oxygen electron centers (POEC; e.g., PO₂-EC, PO₃-EC, PO₄-EC), and oxygen-hole centers (OHC) (Ebeling et al. 2002; He et al. 2017b; He et al. 2018; Petit 2020a). These defects results from the formation and capture of electron and hole pairs during irradiation, and their schematic representations are

shown in Figure 3-1 and Table 3-1 (Ebeling et al. 2002; Fan et al. 2011; Petit 2020a). The POHC defect has single holes trapped on one or a pair of NBO atoms bonded to the same phosphorus whereas POEC has an unpaired electron trapped near the phosphorus in PO₄⁴⁻, PO₃²⁻, and PO₂²⁻ complexes (Ebeling et al. 2002; Fan et al. 2011; Petit 2020a). The generation of radiation-induced defects are dependent on multiple factors including glass composition, intrinsic defects, impurities, and radiation sources (Petit 2020a).

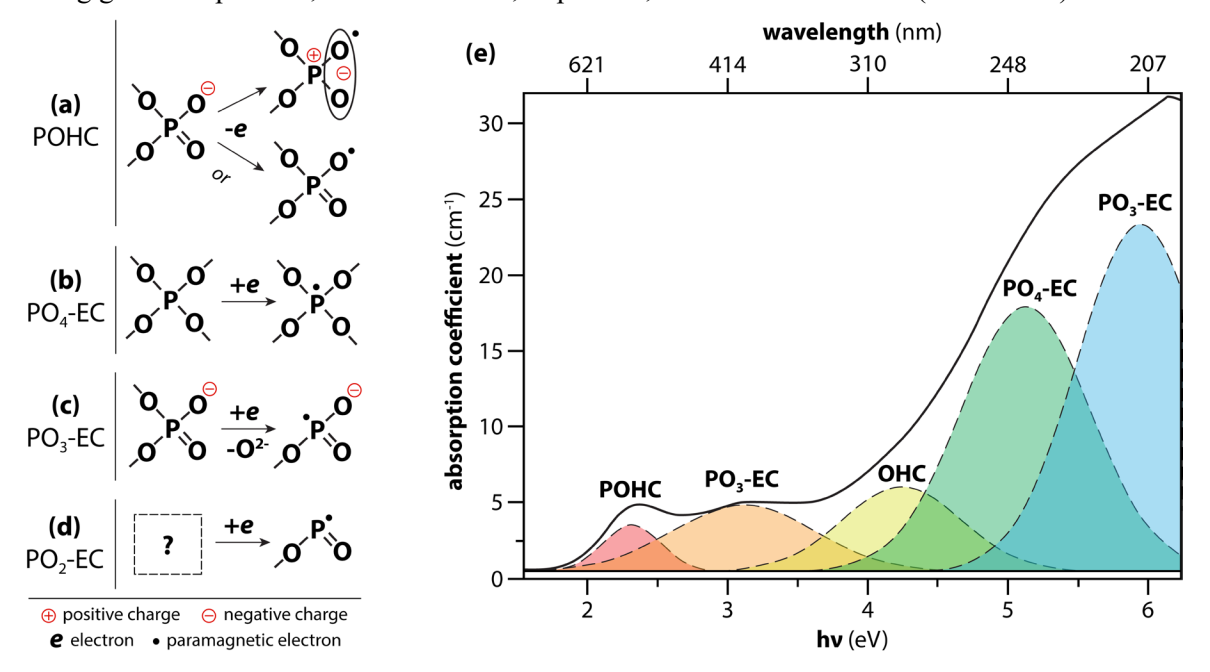


Figure 3-1. (a-d) Schematic representations of some radiation induced defects in phosphate glasses (this figure was modified from the original by Ebeling et al. (2002) and more information about each of these is provided in Table 3-1). (e) Different locations of radiation-induced absorption bands in phosphate glasses in terms of both wavelength and hv including phosphate bonded oxygen hole centers (POHCs), phosphate-related electron centers (PECs), and oxygen related hole centers (OHCs). This figure was modified from the original by He et al. (2017b).

March 19, 2024

Table 3-1. Different types of radiation-induced defects based on a work by Ebeling et al. (2002) including optical information for each (EPR = electron paramagnetic resonance, EC = electron center; HC = hole center).

Defect Type		Standard	EPR parameters(b)	Optical absorption(c)			
Defect	Type	Structure	EFR parameters	λ (nm)	E (eV)	W (eV)	
			W = 1 mT	540	2.30 ± 0.02	0.50	
POHC	НС	Figure 3-1a	$A_{\rm iso} = (4.0 \pm 0.3) \text{ mT}$	430	2.89 ± 0.04	1.00	
			$g_{\rm m} = 2.008 \pm 0.003$	325	3.82 ± 0.04	1.12	
			W = 9 mT		5.12 ± 0.06	1.00	
PO ₄	EC	Figure 3-1b	$A_{\rm iso} = (126 \pm 2) \rm mT$	240			
			$g_{\rm m}$ =2.142 ± 0.008				
	EC		W = 10 mT		5.90 ±0.06	1.00	
PO ₃		Figure 3-1c	$A_{\rm iso} = (86 \pm 2) \text{ mT}$	210			
			$g_{\rm m}$ =2.064 ± 0.005				
			W = 7 mT				
PO_2	EC	Figure 3-1d	$A_{\rm iso} = (27 \pm 2) \mathrm{mT}$	265	4.68 ± 0.08	1.00	
			$g_{\rm m} = 2.006 \pm 0.003$				
ОНС	НС	(a)	W = 7 mT	290	1.20 . 0.06	1.00	
ОПС	пС	(-)	$g = 2.014 \pm 0.001$	_ ∠90	4.28 ± 0.06	1.00	

^(a)Oxygen related center of unknown structure. ^(b)EPR parameters: W is the half amplitude width of the line; $A_{\rm iso}$ is the isotrope hyperfine splitting due to 31 P (distance in mT between two lines), and $g_{\rm m}$ is the middle value between g-values of both lines of a doublet. ^(c)Optical absorption parameters: λ is the wavelength of the band maximum, E is the energy of the band maximum, and W is the half amplitude width of the band.

3.2 Radiation Effects on Phosphate Glasses

In iron phosphate glasses specifically, studies have been conducted looking at radiation stability under different exposures including fluxes of ions (e.g., Kr⁺, Ag⁺, helium ions), γ-rays, ultraviolet (UV) radiation, neutrons, or electrons. Observations of glasses during post-irradiation analysis revealed bubbles, the formation of nanoparticles, phase separation, Fe redox changes (i.e., Fe²⁺/Fe³⁺ ratios), depolymerization, and other structural and/or chemical changes as well as radiation defects discussed in the previous section. A summary of several studies on the radiation effects on phosphate glasses are summarized in Table 3-2 (Shchapova et al. 1995; ElBatal and Ghoneim 1997; Ehrt et al. 1998; Griscom et al. 1998; Ezz-Eldin 1999; Ehrt et al. 2000; Ebeling et al. 2002; Möncke and Ehrt 2004; Sun et al. 2005; Fan et al. 2011; Gandy et al. 2015; Dube et al. 2016; Jolley and Smith 2016; He et al. 2017a; He et al. 2017b; He et al. 2018).

Dube et al. (2016) evaluated radiation damage in iron phosphate glasses with the composition of 60 mol% P_2O_5 and 40 mol% Fe_2O_3 using He ions or Bi ions to simulate radiolysis and ballistic damage effects of α decay from actinides. They discovered that "blisters" of $\sim 1~\mu m$ were observed at a He energy of 30 keV (Figure 3-2). Irradiation from 2 MeV bismuth ions showed that network depolymerization occurred in the form of breakage of Fe–O–P and P–O–P bonds. It is unclear how these types of effects would alter other glass properties such as the chemical durability.

Table 3-2. Summary of some radiation effect studies of the phosphate glasses in the literature.

(a) Simulation only; (b) the exact composition was not provided in the paper; "—" means that the data

was not provided in the primary reference.

	was	not provid	ieu iii tiie p	rimary reference.	
Composition (mol%)	Radiation Source	Energy/ Power (time)	Fluence/ Dose	Irradiation Effects	Ref(s)
(50–60)P ₂ O ₅ , (11– 12)Al ₂ O ₃ , (11–14)MgO, (6– 7)BaO, (2–7)Li ₂ O, (4– 6)K ₂ O, (4)SiO ₂ , (0– 3)H ₃ BO ₃	⁶⁰ Co γ-ray	_	20k, 100k, 250k, 500k, 1000k rad(Si)	Change in transmission spectra was dependent on H ₃ BO ₃ /SiO ₂ ratio, radiation dose, and aging time; charge transfer is closely related to recovery of transmittance and absorption bands of POHC and POEC defects	(He et al. 2017b; He et al. 2018)
(0,10)P ₂ O ₅ , (60,70)LiPO ₃ , (20,30)Al(PO ₃) ₃ , (0,10)Li ₂ CO ₃ , (0,2)AgNO ₃	⁶⁰ Co γ-ray	_	≤ 10 kGy	Formation of POHC and POEC; polyphosphate glass had higher POHC than ultraphosphate and metaphosphate glasses	(Fan et al. 2011)
	He ions	30 keV	2×10 ¹⁷ ions/cm ²	~ 1 μm blisters	(Dube et
	Bi ions	2 MeV	9.2×10 ¹⁴ ions/cm ²	Depolymerization of network in the form of breakage of Fe-O-P and P-O-P bonds	al. 2016)
60P ₂ O ₅ , 40Fe ₂ O ₃	Kr ions	2 MeV	2×10 ¹⁶ ions/cm ²	Reduction of Fe ³⁺ to Fe ²⁺ ; increases in average Fe–O distances; changes in local	(Gandy et al. 2015)
	Au ions	2 MeV	5×10 ¹⁵ ions/cm ²	structure around the Fe ²⁺ and Fe ³⁺ ions	
	(a)	4 keV	_	Molecular dynamics simulation showed a higher [Fe]/[P] atomic ratio resulted in greater displacement after the cascade at 4 keV	(Jolley and Smith 2016)
(40–75)P ₂ O ₅ , (7.5– 40)Fe ₂ O ₃	⁶⁰ Co γ-ray	_	30 MGy	Fe ²⁺ fraction affects the number of defects; possible formation of superoxide ions in the glass structure as radiation-induced defects	(Griscom et al. 1998)
(55–80)P ₂ O ₅ , (20,45)Fe ₂ O ₃ , (0,20)Na ₂ O, 47P ₂ O ₅ , 20Na ₂ O, 31Al ₂ O ₃ , 2K ₂ O	Electron	200 kV	≤ 5×10 ²⁶ e/m ²	All glasses decomposed under 200 keV electron irradiations; migration of alkali elements resulting in P-rich and P-depleted regions in the alkali-containing phosphate glass; formation of bubbles	(Sun et al. 2005)
(50–60)P ₂ O ₅ , (11– 12)Al ₂ O ₃ , (11–14)MgO, (6– 7)BaO, (2–7)Li ₂ O, (4– 6)K ₂ O, (0–4)SiO ₂ , (0– 3)H ₃ BO ₃	⁶⁰ Co γ-ray	-	20k, 100k, 250k, 500k, 1000k rad(Si)	Conversion between Ce ³⁺ and Ce ⁴⁺ by capturing radiation induced holes/electrons reduce POHC and POEC defects; Sb ions functions similar to Ce ions in the glass; Ce and Sb co-doping significantly reduces defects and improve transmission in the visible range	(He et al. 2017a; He et al. 2018)
(50,65)P ₂ O ₅ , (35,50)MO	Xe-Hg lamp	1500 W/m ²	_	Increasing the phosphate decreased the UV radiation resistance and transmission; the	
(M = Mg, Zn, Ca, Ba, Al _{3/2}), (4–20)M(PO ₃) ₂ , (80– 96)AlF ₃ , MF ₂ (M = Mg, Ca, Sr)	KrF laser	70-500 mJ/cm ²	_	concentration ratios of Fe ³⁺ /Fe ²⁺ and P ⁵⁺ /P ³⁺ /P ⁰ in the glass affect the UV absorption and radiation effect; Fe ²⁺ and P ³⁺ suppress the formation of phosphorus-related intrinsic hole centers	(Ehrt et al. 2000)
(4–20)(MF ₂)(PO ₃) ₂ , (80– 96)AlF ₃ , MF ₂ (M = Mg, Ca,	KrF laser	70-500 mJ/cm ² (50 h)	_	Irradiation under KrF laser formed electron centers and hole centers by photoionization of Fe ²⁺ and two-photon mechanism; no defect	(Ehrt et al. 1998)
Sr)	XeHg lamp	1000 W	_	under Xe-Hg lamp; higher phosphate content increased the photoionization rate	

Table 3-2	(continued)
I abic 3-4	Commuca

Composition (mol%)	Radiation Source	Energy/ Power (time)	Fluence/ Dose	Irradiation Effects	Ref(s)
	XeHg lamp	1500 W/m ² (100 h)	_		
100Sr(PO ₃) ₂ , 35AlF ₃ ,	HOK lamp	1500 W/m ² (100 h)	_	Formations of POHC, POEC, and OHC; Fe-	(Möncke
15SrF ₂ , 30CaF ₂ , 10MgF ₂ , 10Sr(PO ₃) ₂	ArF laser	200 mJ/cm ²	_	doped glasses formed the extrinsic defects of Fe-related hole centers	and Ehrt 2004)
1051(1 03)2	KrF laser	200 mJ/cm ²	_	1 c-related note centers	2004)
	Xe-Hg lamp	1000 W	-		
(55,65)P ₂ O ₅ , (3,4)MgO, (9,11)CaO, (9,11)BaO, (4,6)Al ₂ O ₃ , (10,12)ZnO	Cu-Kα X- ray	(≤ 4 h)	_	Formations of POHC, POEC, and OHC; glass melting conditions affects the concentrations of radiation induced defects	(Ebeling et al. 2002)
(50–85)V ₂ O ₅ , (15–50)P ₂ O ₅	γ-ray	-	10 ³ kGy	Changed the internal glass network structures and properties including the polarization, field strength of cations, number of radiation-induced defects, electrical conductivity, and density; increasing P ₂ O ₅ increased the Vickers microhardness but decreased the electrical conductivity	(Ezz-Eldin 1999)
~80P ₂ O ₅ , 20Na ₂ O, 0.5V ₂ O ₅	⁶⁰ Co γ-ray		<10 ⁴ Gy	V ions helps the formation or suppression of color centers	(ElBatal and Ghoneim 1997)
BeO, P ₂ O ₅ (b)	Neutron	1 MeV	4.5×10 ¹⁷ ions/cm ²	Deformed both short- and middle-range order in the glass; decreased P–O and P–P distance while increasing P–O–P angle.	(Shchapov a et al. 1995)

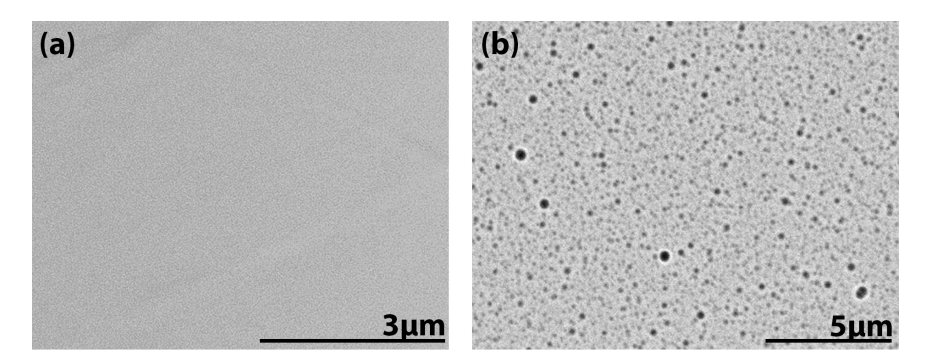


Figure 3-2. Scanning electron micrographs of iron phosphate glasses showing (a) as-made samples and (b) after He ion irradiation on a pre-damaged specimen. This figure was modified from the original by Dube et al. (2016).

In a separate study by Gandy et al. (2015), analysis of 60 mol% P_2O_5 and 40 mol% Fe_2O_3 glasses irradiated with 2 MeV Kr^+ or Au^+ ions showed additional damages to the glasses. To assess the progress of damage, X-ray absorption spectroscopy was performed looking at the Fe-K edge. Here, radiation-induced damage was observed in the form of (1) Fe^{3+} reduction to Fe^{2+} , (2) increases in average Fe–O distances, and (3) changes in local structure around the Fe^{2+} and Fe^{3+} ions.

Griscom et al. (1998) investigated the structural changes in iron phosphate glasses containing 40–75 mol% P₂O₅ and 7.5–40 mol% Fe₂O₃ with other minor constituents under gamma ray does of 30 MGy using

electron spin resonance. They showed that the fraction of Fe^{2+} is dependent on the melting conditions and batch composition, and the Fe^{2+} fraction affects the number of defects in the glass structure. Their results indicated the possible formation of superoxide ions in the glass structure as radiation-induced defects during gamma irradiation.

Sun et al. (2005) studied the effects of electron irradiation on iron phosphate glasses with (55, 60, 80 mol%) P₂O₅, (20, 45 mol%) Fe₂O₃, (0, 20 mol%) Na₂O, and aluminophosphate with 46.5 mol% P₂O₅, 20.2 mol% Na₂O, 31.5 mol% Al₂O₃, and 1.8 mol% K₂O along with sodium borosilicate glasses. The synthesized glasses were characterized with transmission electron microscopy, and they discovered that all the glasses decomposed under 200 kV electron irradiation. Irradiation induced the migration alkali elements resulting in phosphorous-rich and -depleted regions in all alkali-containing glasses. Figure 3-3 shows the TEM images of iron phosphate glasses after irradiations, as well as elemental maps of Fe, P, and O of aluminophosphate glasses after irradiation. Formation of bubbles occurred on the Na-containing iron phosphate and aluminophosphate glasses but not in borosilicate glasses.

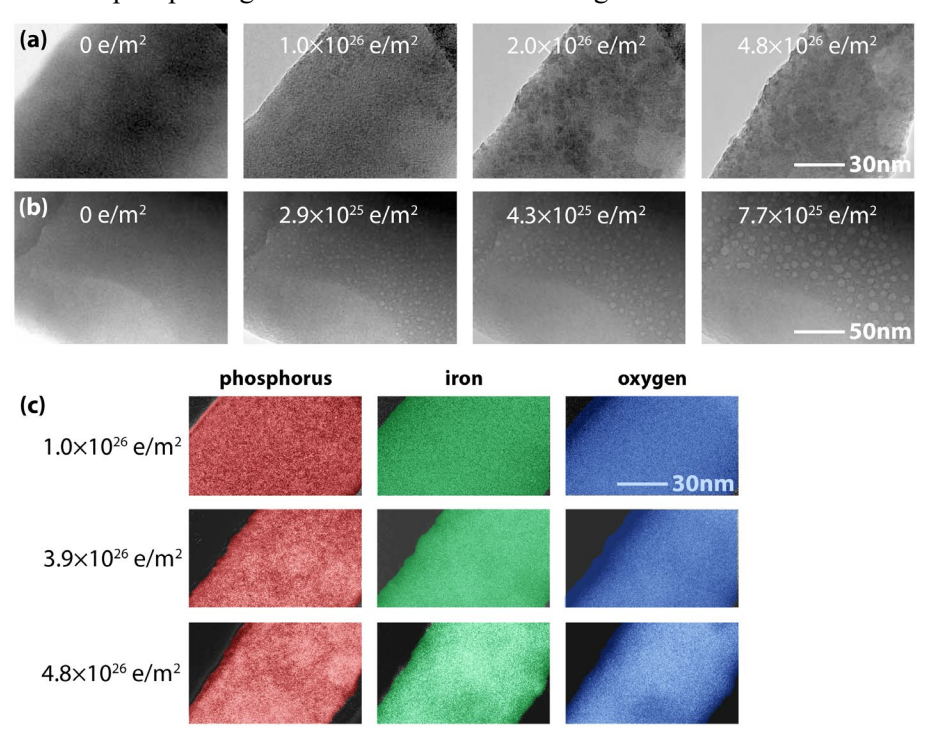


Figure 3-3. (a,b) Bright-field transmission electron micrographs (TEM) on iron phosphate glasses without Na in the structure (a) and with Na in the structure (b) after irradiation by electron beam at different doses. (c) Pseudocolored elemental energy dispersive X-ray spectroscopy dot maps of P, Fe, and O using energy-filtered TEM on aluminophosphate glass irradiated to different electron doses. This figure was modified from the original by Sun et al. (2005).

A molecular dynamics study by Jolley and Smith (2016) on the iron phosphate glasses with 60 mol% P_2O_5 and 40 mol% Fe_2O_3 showed that glasses with higher [Fe]/[P] atomic ratios had greater displacement after the cascade at 4 keV and were more vulnerable to radiation damage. The PO_4 polyhedra were destroyed but recovered in the early stages of irradiation.

Fan et al. (2011) investigated the defect centers induced by γ radiation in phosphate glasses synthesized with 0 or 10 mol% P₂O₅, 60 or 70 mol% LiPO₃, 20 or 30 mol% Al(PO₃)₃, 0 or 10 mol% Li₂CO₃, and 0 or 2 mol% AgNO₃. Three types of phosphate glasses including polyphosphate ([O]/[P] = 3.07), metaphosphate ([O]/[P] = 3), and ultraphosphate ([O]/[P] = 2.93) glasses were either doped with silver or were left undoped, and the glasses were characterized using electron paramagnetic resonance (EPR) and optical

absorption spectra. Gamma radiation formed POHC and POEC. The undoped polyphosphate and ultraphosphate glasses showed better UV transmittance after irradiation compared to undoped metaphosphate glass. They found that Ag⁺ trapping hole is the main reason of the stabilization phenomenon of radio-photoluminescence centers. Polyphosphate glasses had higher POHC than ultraphosphate and metaphosphate glasses.

He et al. (2017b) studied the defects in the phosphate glasses from gamma radiation. Phosphate glasses with batched compositions of 50–60 mol% P₂O₅, 11–12 mol% Al₂O₃, 11–14 mol% MgO, 6–7 mol% BaO, 2–7 mol% Li₂O, 4–6 mol% K₂O, 4 mol% SiO₂, and 0–3 mol% H₃BO₃ were investigated to understand the effects of the H₃BO₃/SiO₂ mass ratio on the recovery of radiation induced defects. Changes in transmission spectra were dependent on H₃BO₃/SiO₂ mass ratio, radiation dose, and aging times (Figure 3-4). They observed that charge transfer was closely related to the recovery of transmittance and absorption bands of POHC and EC defects (He et al. 2017b).

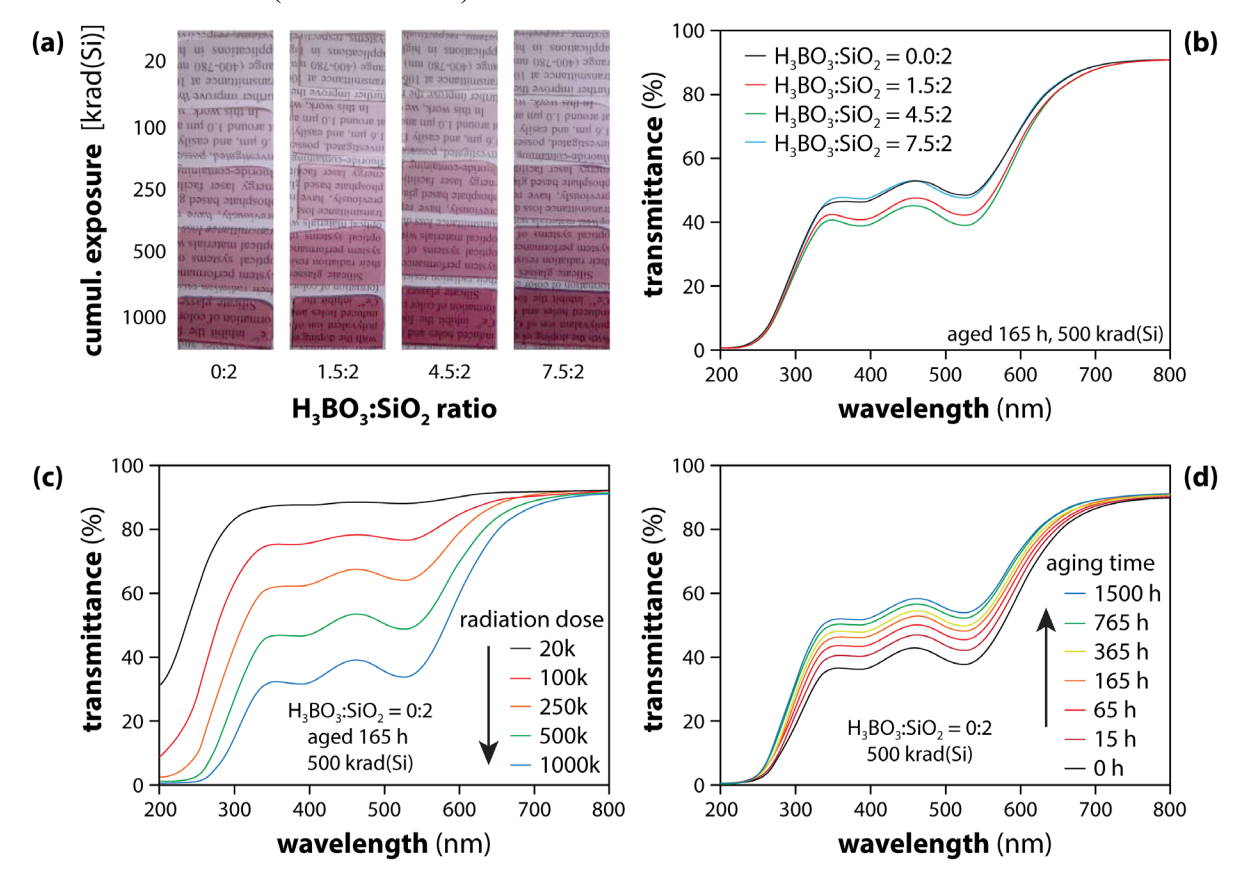


Figure 3-4. (a) Photographs of a series of phosphate-based glasses with different H₃BO₃:SiO₂ mass ratio (0:2, 1.5:2, 4.5:2 and 7.5:2) after exposure to different cumulative (cumul.) radiation doses of 20, 100, 250, 500, or 1000 krad(Si). (b) Transmittance spectra of the series of glasses with different mass ratios of H₃BO₃:SiO₂ (see above) after γ irradiations of 500k rad(Si) after being aged for 165 h. (c) transmittance spectra of the H₃BO₃:SiO₂ = 0:2 sample after irradiations of 20, 100, 250, 500, and 1000 krad(Si) with an aging time of 165 h. (d) Transmittance spectra of the sample (H₃BO₃:SiO₂ = 0:2) with γ radiation of 500 krad(Si) after different aging times of 0, 15, 65, 165, 365, 765, or 1500 h at room temperature. This figure was modified from the original by He et al. (2017b).

In another study, He et al. (2017a) investigated the effects of Sb_2O_3 and CeO_2 co-doping on the γ radiation resistance in phosphate glasses comprised of 50–60 mol% P_2O_5 , 11–12 mol% Al_2O_3 , 11–14 mol% MgO_5

6–7 mol% BaO, 2–7 mol% Li₂O, 4–6 mol% K₂O, 0–4 mol% SiO₂, and 0–3 mol% H₃BO₃. The Ce ions are generally present as Ce⁴⁺ in the glasses but can be converted to Ce³⁺ by capturing radiation-induced electrons, resulting in decrease of EC defects. Similarly, Ce³⁺ can convert to Ce⁴⁺ by capturing radiation induced holes and inhibits the formation of POHC. The Ce ions also reduces the number of NBO atoms and consequently decreases POHC and EC defects. The Sb ions functioned similarly as Ce in the phosphate glasses. The Sb and Ce co-doped phosphate glasses showed the significant resistance to γ radiation and great improvement in transmittance within the visible range.

Ehrt et al. (2000) correlated the basicity of the glass and the redox states of Fe and P cations to the UV radiation resistance and transmission. Ultraphosphate glasses with 65 mol% P_2O_5 -35 mol% MO (M = Mg, Zn, Ca, Ba, Al_{3/2}), metaphosphate 50 mol% P_2O_5 -50 mol% MO (M = Mg, Zn, Ca, Ba, Al_{3/2}), and fluoride-phosphate glasses with 4–20 mol% of M(PO₃)₂ (M = Mg, Ca, Sr, Ba, Zn, Pb) and 80–96 mol% of AlF₃ and MF₂ (M = Mg, Ca, Sr) were synthesized and characterized with EPR. The Fe content was either added or present as impurity in the chemicals, and its concentration was in the ppm range. Increasing phosphate content in the glass decreased the UV radiation resistance and transmission. The concentration ratios of Fe³⁺/Fe²⁺ and P⁵⁺/P³⁺/P⁰ in the glass affect the UV absorption and radiation effects. The photoionization of Fe²⁺ by single-photo mechanism forms stable (Fe²⁺)⁺ and electron centers whereas Fe²⁺ and P³⁺ suppress the formation of intrinsic hole centers related to phosphorus.

In a similar study, Ehrt et al. (1998) investigated the radiation damage on the ultraphosphate and fluoride phosphate glasses containing 4–20 mol% of M(PO₃)₂ and 80–96 mol% of AlF₃ and MF₂ under a Xe-Hg lamp and KrF excimer laser by analyzing the radiation-induced absorption spectra (it should be noted that M was not specified in this study, but from their previous study (Ehrt et al. 2000), M likely includes Mg, Zn, Ca, Ba, Al, and Sr). Here, they showed that reducing and oxidizing conditions during melting affected the Fe²⁺/Fe³⁺ redox ratio in the final glass (Ehrt et al. 1998). The glasses melted under reducing conditions had higher Fe²⁺, and the photoionization of Fe²⁺ occurred by a single-photon mechanism during radiation, leading to defects; the photoionization rate increased with higher phosphate content. This study showed that the photoionization rate is relatively low for fluoride phosphate glasses compared to ultraphosphate glass (Ehrt et al. 1998).

The effects of glass matrix, irradiation source, and dopants on the phosphate and borosilicate glasses were investigated by Möncke and Ehrt (2004). The phosphate glass of Sr(PO₃)₂ and fluoride-phosphate glass of 35 mol% AlF₃, 15 mol% SrF₂, 30 mol% CaF₂, 10 mol% MgF₂, and 10 mol% Sr(PO₃)₂ were irradiated with a Xe-Hg lamp, a high-pressure Hg (HOK) lamp, an ArF laser, and a KrF laser. The irradiation defects are categorized as *intrinsic defects* whereas the defects related to the ionization of dopants are categorized as *extrinsic defects*. Both phosphate and fluoride-phosphate glasses formed similar intrinsic defects including POHCs, phosphate-related electron centers (PECs), and OHCs after irradiation. The Fe-doped glasses formed the extrinsic defects of Fe-related hole centers, and the photoionization of Fe was observed. The type of irradiation sources affected the formation of intrinsic defects, but further studies were needed to clarify. They found that the formation of extrinsic defects can cause an increase of intrinsic defects. Comparing the effects of dopants including Co, Fe, Mn, and Ni, ions with higher electronegativities increased the photooxidation (Möncke and Ehrt 2004).

Ebeling et al. (2002) studied the X-ray-induced effects in phosphate glass using a Cu-K α X-ray source. The ultraphosphate glass with 65.3 mol% P_2O_5 , 3.2 mol% MgO, 8.8 mol% CaO, 8.6 mol% BaO, 4.4 mol% Al_2O_3 , 9.7 mol% ZnO and metaphosphate glass with 55.6 mol% P_2O_5 , 4.1 mol% MgO, 11.4 mol% CaO, 10.9 mol% BaO, 5.6 mol% Al_2O_3 , and 12.4 mol% ZnO were irradiated for 10–240 min. In both glasses, POHCs, POECs, and OHCs were present after irradiation, and the melting conditions affected the concentrations of irradiation induced defects in the glass.

Ezz-Eldin (1999) evaluated the radiation effects on glasses with 50–85 mol% V_2O_5 and 15–50 mol% P_2O_5 glasses under a γ irradiation dose of 1 MGy. The vanadium ions in the glass were in mixed valence states as V^{3+} , V^{4+} , and V^{5+} depending on the composition of the glass. The γ irradiation changed the internal glass

network structures and properties including the polarizations, cation field strengths, number of radiation-induced defects, electrical conductivities, and densities (Ezz-Eldin 1999). Increasing P₂O₅ contents resulted in increased softening points and Vickers microhardness values whereas the electrical conductivities and densities generally decreased after irradiation (Ezz-Eldin 1999).

ElBatal and Ghoneium (1997) showed that vanadium ions in the vanadium-doped sodium phosphate glasses (\sim 80 mol% P_2O_5 , 20 mol% Na_2O , and 0.5 mol% V_2O_5) affected the formation of radiation induced defects. In phosphate glasses, vanadium ions generally exist in lower valence states among the possible states of V^{3+} , V^{4+} , and V^{5+} . The vanadium ions with three different oxidation states provide alternate sites that may initiate or impede the formation of color centers.

Shchapova et al. (1995) investigated the structural changes of beryllium phosphate glasses after neutron irradiation of 1 MeV and flux of 4.5×10^{17} cm⁻². The results showed that irradiation of fast neutrons deformed both SRO and MRO structures of BeO–P₂O₅ glass. Neutron irradiation increased number of NBO atoms and decreased the average distances of P–O and P–P due to breakage of glass networking (Shchapova et al. 1995). The angle of P–O–P increased as well, and the structural parameters after irradiation were similar to ultraphosphate glass. The initial quartz like structure of BeO–P₂O₅ glass transformed into glass with ultraphosphate and polyphosphate compositions after irradiation (Shchapova et al. 1995).

Stefanovsky et al. (2016) reported the effect of 8 MeV electron irradiation on the structure of sodium aluminum (iron) phosphate glasses (40 mol% Na₂O, (20-X) mol% Al₂O₃, X mol% Fe₂O₃, 40 mol% P₂O₅) which were used in Russia for HLW. No appreciable changes in the structure of anionic motif of the glass network and in the oxidation state and coordination environment of iron up to a dose of 1.0 MGy.

Luzhetsky et al. (2020) investigated structural evolution and water dissolution of sodium-aluminophosphate (NAP) nuclear waste glasses under gamma irradiation from ⁶⁰Co source. A comparison of pristine and irradiated glasses with a dose of 62 MGy, the leaching rate of elements from irradiated NAP glasses was averagely decreased by approximately two times.

4. SUMMARY AND CONCLUSIONS

This paper summarizes some of the original work as well as recent work on phosphate glasses including the composition-property relationships, phosphate glass structure, and radiation stability of phosphate glasses. The chemical durability of phosphate glasses can vary over many orders of magnitude with small compositional changes in a given system such as the P₂O₅-Fe₂O₃ binary system, the [Fe]/[P] ratio, the [O]/[P] ratio, as well as the Fe²⁺/Fe³⁺ redox ratio. Irradiation studies of phosphate glasses showed a range of effects including electron-induced alkali migration and bubble formation due to neutron-induced increases in NBOs and broken P–O bonds. These types of changes to glass structure will likely result in changes to the chemical durability of these glasses. This should be explored in more detail in future studies. Finding an effective waste form requires simultaneous optimization of many properties including the waste loading, the composition, the chemical durability, and thermal properties. In some cases, crystals can form during cooling following waste form production. Understanding the impacts that the new phases have on the final chemical durability and radiation stability of the final waste form is important.

5. ACKNOWLEDGEMENTS

Pacific Northwest National Laboratory is operated by Battelle Memorial Institute for the DOE under contract DE-AC05-76RL01830. This report is dedicated to Ted Day, formerly of the Mo-Sci Corporation. MT, SC, JM, and BR acknowledge funding support from the Department of Energy Office of Nuclear Energy's Nuclear Technology Research and Development Program. This report summarizes some of the work done in a joint collaboration between PNNL, MoSci Corporation, Missouri University of Science and Technology, and Clemson University (where Professor Ming Tang was before he joined DOE-NE as a Federal Manager) that was presented during the Phosphate Round Table Workshop held jointly by PNNL and Argonne National Laboratory in August 2020. Authors express thanks to William Ebert of ANL for support as well as Ken Marsden (Idaho National Laboratory) and Kimberly Gray (DOE-NE) for programmatic support.

6. REFERENCES

Ahmed, I. 2019. "Developing unique geometries of phosphate-based glasses and their prospective biomedical applications." **63**(1):34-42.

Bai, J, RK Brow, and C Kim. 2020. "Redox effects on the structure and properties of Na-Mo-Fe phosphate glasses." *Journal of Non-Crystalline Solids* **557**.

Bingham, PA and ER Barney. 2012. "Structure of iron phosphate glasses modified by alkali and alkaline earth additions: neutron and x-ray diffraction studies." *J Phys Condens Matter* **24**(17):175403.

Brezneva, NE, AA Minaev, and SN Oziraner. 1979. Vitrification of high sodium-aluminum wastes: Composition ranges and properties. In *Proceedings of MRS Proc.* eds. M G.J., vol. 1, pp. 43-50, Plenum Press, New York.

Brow, RK. 2000. "Review: the structure of simple phosphate glasses." *Journal of Non-Crystalline Solids* **263-264**:1-28.

Brow, RK, CW Kim, and ST Reis. 2019. "Iron polyphosphate glasses for waste immobilization." *International Journal of Applied Glass Science* **11**(1):4-14.

Brow, RK, DR Tallant, JJ Hudgens, SW Martin, and AD Irwin. 1994. "The short-range structure of sodium ultraphosphate glasses." *Journal of Non-Crystalline Solids* 177:221-28.

Brow, RK, DR Tallant, ST Myers, and CC Phifer. 1995. "The short-range structure of zinc polyphosphate glass." *Journal of Non-Crystalline Solids* **191**(1-2):45-55.

Cotton, FA and G Wilkinson. 1980. *Advanced Inorganic Chemistry*, 4th ed., John Wiley & Sons, New York, NY.

Day, D, E. and CS Ray. 2013. A Review of Iron Phosphate Glasses and Recommendations for Vitrifying Hanford Waste. INL/EXT-13-30839, Idaho National Laboratory, Idaho Falls, ID.

Day, DE, Z Wu, CS Ray, and P Hrma. 1998. "Chemically durable iron phosphate glass wasteforms." *Journal of Non-Crystalline Solids* **241**(1):1-12.

Dube, CL and NC Hyatt. 2019. Investigation of Radiation Damage in Iron Phosphate Glasses by Soft X-Ray Absorption Spectroscopy: A Powerful Tool for Surface Characterization. In *Proceedings* pp. 133-39, Springer Singapore.

Dube, CL, MC Stennett, S Akhmadaliev, and NC Hyatt. 2020. "Investigation of ion irradiation induced damages in iron phosphate glasses: Role of electronic and nuclear losses in glass network modification." *Journal of Non-Crystalline Solids:* X **8**:100055.

Dube, CL, MC Stennett, AS Gandy, and NC Hyatt. 2016. "Simulation of alpha decay of actinides in iron phosphate glasses by ion irradiation." *Nuclear Instruments and Methods in Physics Research Section B: Beam Interactions with Materials and Atoms* **371**:424-28.

Ebeling, P, D Ehrt, and M Friedrich. 2002. "X-ray induced effects in phosphate glasses." *Optical Materials* **20**(2):101-11.

- Ebert, WL and JA Fortner. 2019. *Analysis of iron phosphate glasses for dehalogenated salt waste*. ANL/CFCT-19/5 153602, Argonne National Laboratory, Lemont, IL.
- Ehrt, D, P Ebeling, and U Natura. 2000. "UV Transmission and radiation-induced defects in phosphate and fluoride—phosphate glasses." *Journal of Non-Crystalline Solids* **263**:240-50.
- Ehrt, D, U Natura, P Ebeling, and M Müller. 1998. Formation and healing of UV radiation defects in phosphate and fluoride phosphate glasses with high UV transmission. In *Proceedings of Proc. XVIII International Congress on Glass, San Francisco, CA (USA)*. pp. 1-6.
- ElBatal, H and N Ghoneim. 1997. "Absorption spectra of gamma-irradiated sodium phosphate glasses containing vanadium." *Nuclear Instruments and Methods in Physics Research Section B: Beam Interactions with Materials and Atoms* **124**(1):81-90.
- Ezz-Eldin, F. 1999. "Radiation effects on some physical and thermal properties of V₂O₅–P₂O₅ glasses." Nuclear Instruments and Methods in Physics Research Section B: Beam Interactions with Materials and Atoms **159**(3):166-75.
- Fan, S, C Yu, D He, K Li, and L Hu. 2011. "Gamma rays induced defect centers in phosphate glass for radio-photoluminescence dosimeter." *Radiation measurements* **46**(1):46-50.
- Fletcher, LB, JJ Witcher, N Troy, ST Reis, RK Brow, and DM Krol. 2011. "Direct femtosecond laser waveguide writing inside zinc phosphate glass." *Optics Express* **19**(9):7929-36.
- Gandy, A, MC Stennett, C Brigden, and NC Hyatt. 2015. Ion beam irradiation induced structural modifications in iron phosphate glasses: A model system for understanding radiation damage in nuclear waste glasses. In *Proceedings of Materials Research Society*. vol. 1757, Materials Research Society.
- Gin, S, A Abdelouas, LJ Criscenti, WL Ebert, K Ferrand, T Geisler, MT Harrison, Y Inagaki, S Mitsui, KT Mueller, JC Marra, CG Pantano, EM Pierce, JV Ryan, JM Schofield, CI Steefel, and JD Vienna. 2013. "An international initiative on long-term behavior of high-level nuclear waste glass." *Materials Today* **16**(6):243-48.
- Griscom, D, C Merzbacher, N Bibler, H Imagawa, S Uchiyama, A Namiki, G Marasinghe, M Mesko, and M Karabulut. 1998. "On the structure and radiation chemistry of iron phosphate glasses: New insights from electron spin resonance, Mössbauer, and evolved-gas mass spectroscopy." *Nuclear Instruments and Methods in Physics Research Section B: Beam Interactions with Materials and Atoms* **141**(1-4):600-15.
- He, Q, P Wang, M Lu, and B Peng. 2018. "The Nature of the Defects in Phosphate-Based Glasses Induced by Gamma Radiation." In *Advances in Glass Science and Technology*, IntechOpen.
- He, Q, P Wang, M Sun, M Lu, and B Peng. 2017a. "Significant improvement of gamma radiation resistance in CeO₂ doped phosphate glass by co-doping with Sb₂O₃." *Optical Materials Express* 7(3):1113-21.
- He, Q, Y Xue, P Wang, M Sun, M Lu, and B Peng. 2017b. "Natural healing behavior of gamma radiation induced defects in multicomponent phosphate glasses used for high energy UV lasers." *Optical Materials Express* 7(9):3284-93.
- Heng, X, Q Qian, X Chen, L Liu, X Zhao, D Chen, and Z Yang. 2015. "Reduced radiation damage in a multicomponent phosphate glass by Nb⁵⁺ or Sb³⁺ doping." *Optical Materials Express* **5**(10):2272-80.

Jolley, K and R Smith. 2016. "Iron phosphate glasses: structure determination and radiation tolerance." *Nuclear Instruments and Methods in Physics Research Section B: Beam Interactions with Materials and Atoms* **374**:8-13.

Keen, DA. 2001. "A comparison of various commonly used correlation functions for describing total scattering." *Journal of Applied Crystallography* **34**:172-77.

Kim, D-S, WC Buchmiller, MJ Schweiger, JD Vienna, DE Day, C-W Kim, D Zhu, TE Day, T Neidt, DK Peeler, TB Edwards, IA Reamer, and RJ Workman. 2003. *Iron Phosphate as an Alternative Waste-Form for Hanford LAW*. PNNL-14251, Pacific Northwest National Laboratory, Richland, WA.

Kurkjian, CR and WR Prindle. 2005. "Perspectives on the History of Glass Composition." *Journal of the American Ceramic Society* **81**(4):795-813.

Lim, JW, SW Yung, and RK Brow. 2011. "Properties and structure of binary tin phosphate glasses." *Journal of Non-Crystalline Solids* **357**(14):2690-94.

Luzhetsky, AV, VA Petrov, SV Yudintsev, VI Malkovsky, MI Ojovan, MS Nickolsky, AA Shiryaev, SS Danilov, and EE Ostashkina. 2020. "Effect of Gamma Irradiation on Structural Features and Dissolution of Nuclear Waste Na–Al–P Glasses in Water." *Sustainability* **12**(10):4137.

Ma, L and RK Brow. 2014. "Structural study of Na₂O–FeO–Fe₂O₃–P₂O₅ glasses by high-pressure liquid chromatography." *Journal of Non-Crystalline Solids* **387**:16-20.

Ma, L, RK Brow, and ME Schlesinger. 2017. "Dissolution behavior of Na₂O–FeO–Fe₂O₃–P₂O₅ glasses." *Journal of Non-Crystalline Solids* **463**:90-101.

Ma, L, RK Brow, and ME Schlesinger. 2018. "Dissolution behaviour of sodium calcium polyphosphate glasses." *Physics and Chemistry of Glasses: European Journal of Glass Science and Technology Part B* **59**(5):205-12.

Magnien, V, DR Neuville, L Cormier, J Roux, JL Hazemann, O Pinet, and P Richet. 2006. "Kinetics of iron redox reactions in silicate liquids: A high-temperature X-ray absorption and Raman spectroscopy study." *Journal of Nuclear Materials* **352**(1-3):190-95.

Möncke, D and D Ehrt. 2004. "Irradiation induced defects in glasses resulting in the photoionization of polyvalent dopants." *Optical Materials* **25**(4):425-37.

Onodera, Y, S Kohara, H Masai, A Koreeda, S Okamura, and T Ohkubo. 2017. "Formation of metallic cation-oxygen network for anomalous thermal expansion coefficients in binary phosphate glass." *Nature Communications* **8**:15449.

Park, H-S, I-T Kim, Y-Z Cho, H-C Eun, and H-S Lee. 2008. "Stabilization/solidification of radioactive salt waste by using xSiO₂–yAl₂O₃–zP₂O₅ (SAP) material at molten salt state." *Environmental Science & Technology* **42**(24):9357-62.

Perez, JM, DF Bickford, DE Day, DS Kim, SL Lambert, SL Marra, DK Peeler, DM Strachan, MB Triplett, JD Vienna, and RS Wittman. 2001. *High-Level Waste Melter Study Report*. PNNL-13582, Pacific Northwest National Laboratory, Richland, WA.

Petit, L. 2020a. "Radiation effects on phosphate glasses." *International Journal of Applied Glass Science* **11**(3):511-21.

Petit, L. 2020b. "Radiation effects on phosphate glasses: Review." *International Journal of Applied Glass Science* **11**(3):511-21.

Riley, BJ and S Chong. 2020. "Glass waste form options for rare-earth fission products from electrochemical reprocessing." *Journal of Non-Crystalline Solids* **545**:120161.

Riley, BJ, JA Peterson, JD Vienna, WL Ebert, and SM Frank. 2020. "Dehalogenation of electrochemical processing salt simulants with ammonium phosphates and immobilization of salt cations in an iron phosphate glass waste form." *Journal of Nuclear Materials* **529**:151949.

Riley, BJ, JD Vienna, and WL Ebert. 2021. *Road Map for Developing Iron Phosphate Waste Forms for Salt Wastes*. PNNL-30998, ANL/CFCT-20/44, Pacific Northwest National Laboratory, Richland, WA.

Sales, BC and LA Boatner. 1984a. "Lead phosphate glass as a stable medium for the immobilization and disposal of high-level nuclear waste." *Materials Letters* **2**(4, Part B):301-04.

Sales, BC and LA Boatner. 1984b. "Lead-iron phosphate glass: a stable storage medium for high-level nuclear waste." *Science* **226**(4670):45-48.

Sales, BC, JU Otaigbe, GH Beall, LA Boatner, and JO Ramey. 1998. "Structure of zinc polyphosphate glasses." *Journal of Non-Crystalline Solids* **226**(3):287-93.

Shchapova, JV, A Zatsepin, and AM Nepomiluev. 1995. "Neutron induced damages of short- and middle-range order structure in berillium phosphate glasses." In *Proceedings of XVII International Congress on Glass*, Vol 2, pp. 359-62. Chinese Ceramic Society, Beijing.

Siemer, DD. 2012. "Improving the integral fast reactor's proposed salt waste management system." *Nuclear Technology* **178**(3):341-52.

Song, K-C, H-S Lee, J-M Hur, J-G Kim, D-H Ahn, and Y-Z Cho. 2010. "Status of pyroprocessing technology development in Korea." *Nuclear Engineering and Technology* **42**(2):131-44.

Stefanovsky, SV, IA Presniakov, AV Sobolev, IS Glazkova, MI Kadyko, and OI Stefanovsky. 2016. "The effect of electron irradiation on the structure and iron speciation in sodium aluminum (iron) phosphate glasses." *Journal of Nuclear Materials* **476**:262-69.

Stefanovsky, SV, OI Stefanovskaya, SE Vinokurov, SS Danilov, and BF Myasoedov. 2015a. "Phase composition, structure, and hydrolytic durability of glasses in the Na₂O-Al₂O₃-(Fe₂O₃)-P₂O₅ system at replacement of Al₂O₃ by Fe₂O₃." *Radiochemistry* **57**(4):348-55.

Stefanovsky, SV, OI Stefanovsky, SS Danilov, and MI Kadyko. 2019. "Phosphate-based glasses and glass ceramics for immobilization of lanthanides and actinides." *Ceramics International* **45**(7, Part B):9331-38.

Stefanovsky, SV, OI Stefanovsky, MI Kadyko, IA Presniakov, and BF Myasoedov. 2015b. "The effect of Fe₂O₃ substitution for Al₂O₃ on the phase composition and structure of sodium-aluminum-iron phosphate glasses." *Journal of Non-Crystalline Solids* **425**:138-45.

Stefanovsky, SV, OI Stefanovsky, MB Remizov, PV Kozlov, EA Belanova, RA Makarovsky, and BF Myasoedov. 2017. "Sodium-aluminum-iron phosphate glasses as legacy high level waste forms." *Progress in Nuclear Energy* **94**:229-34.

Sun, K, L Wang, RC Ewing, and WJ Weber. 2005. "Effects of electron irradiation in nuclear waste glasses." *Philosophical Magazine* **85**(4-7):597-608.

Vienna, JD, ED Collins, JV Crum, WL Ebert, SM Frank, TG Garn, D Gombert, R Jones, RT Jubin, VC Maio, JC Marra, J Matyas, TM Nenoff, BJ Riley, GJ Sevigny, NR Soelberg, DM Strachan, PK Thallapally, and JH Westsik. 2015. *Closed Fuel Cycle Waste Treatment Strategy*. FCRD-MRWFD-2015-000674, PNNL-24114, Pacific Northwest National Laboratory, Richland, WA.

Vienna, JD, JV Ryan, S Gin, and Y Inagaki. 2013. "Current understanding and remaining challenges in modeling long-term degradation of borosilicate nuclear waste glasses." *International Journal of Applied Glass Science* **4**(4):283-94.

Wright, AC, RN Sinclair, JL Shaw, R Haworth, GK Marasinghe, and DE Day. 2008. "A neutron diffraction study of the structure of iron phosphate glasses." *Physics and Chemistry of Glasses* 7:1-7.

Yamauchi, H, G Park, T Nagakane, T Honma, T Komatsu, T Sakai, and A Sakamoto. 2013. "Performance of Lithium-Ion Battery with Tin-Phosphate Glass Anode and Its Characteristics." *Journal of the Electrochemical Society* **160**(10):A1725-A30.

Yu, X, DE Day, GJ Long, and RK Brow. 1997. "Properties and structure of sodium-iron phosphate glasses." *Journal of Non-Crystalline Solids* **215**(1):21-31.